JAERI-M
92-136

COMPARATIVE STUDY OF LOW AND HIGH ASPECT RATIO DEVICES FOR ITER DESIGN OPTIONS

September 1992

Masayoshi SUGIHARA, Eisuke TADA
Yasuo SHIMOMURA, Toshihide TSUNEMATSU
Satoshi NISHIO, Toshiko NAKAZATO*
Yoshiki MURAKAMI*, Koichi KOIZUMI
and ITER Project Team

日本原子力研究所
Japan Atomic Energy Research Institute

JAERI-Mレポートは，日本原子力研究所が不定期に公刊している研究報告書です。
入手の問合わせは，日本原子力研究所技術情報部情報資料課（〒319－11茨城県那珂郡東海村）あて，お申しこしください。なお，このほかに財団法人原子力弘済会資料センター（〒319-11茨城県那珂郡東海村日本原子力研究所内）で複写による実費頒布をおこなっております。

JAERI-M reports are issued irregularly.
Inquiries about availability of the reports should be addressed to Information Division, Department of Technical Information, Japan Atomic Energy Research Institute, Tokai-mura, Naka-gun, Ibaraki-ken 319-11, Japan.

編集兼発行　日本原子力研究所
印　　刷　日立高速印刷株式会社

JAERI-M 92-136

Comparative Study of Low and High Aspect Ratio Devices for ITER Design Options

Masayoshi SUGIHARA, Eisuke TADA, Yasuo SHIMOMURA
Toshihide TSUNEMATSU, Satoshi NISHIO, Toshiko NAKAZATO*
Yoshiki MURAKAMI*, Koichi KOIZUMI and ITER Project Team

Department of ITER Project
Naka Fusion Research Establishment
Japan Atomic Energy Research Institute
Naka-machi, Naka-gun, Ibaraki-ken

(Received August 14, 1992)

Comparative study on the plasma performance and the engineering characteristics of low and high aspect ratio devices for ITER (International Thermonuclear Experimental Reactor) design option is done to examine quantitatively the expected merit and demerit of high aspect ratio device on steady state operation. Device parameters of aspect ratio A=3 and 4 are chosen for comparative study with same confinement capability for ignition based on ITER-power scaling law. Improvement of steady state operation with A=4 is found only moderate, e.g. Q and bootstrap fraction increased by about 1 and 10%, respectively, when A is increased from 3 to 4. Reduction of stability margin in vertical instability is about 20% and plasma elongation must be decreased from 2 down to about 1.8 to recover this reduction of stability margin with A=4. If such lower elongation is employed, single null divertor configuration should be employed to reduce the capacity of poloidal field system. Detailed 2D divertor code calculation shows that peak heat load per unit area of A=4 device with SN configuration increases compared with A=3 device with DN configuration, contrary to the predictions so far made. Large

---

* On leave from Toshiba Corporation

experimental capability to obtain the data base for demo-reactor (e.g., high Q with high bootstrap fraction) can be expected even in A=3 device when the extended plasma performance could be realized. Similar overall performance in the future commercial reactor with steady state operation is expected even in A=3 device compared with A=4 device by adjusting the fusion power.

Preliminary engineering studies indicate that A=4 device would have less space for handling the in-vessel components and doubled toroidal field magnet weight and winding length, and hence is less desirable when compared with the present ITER design (A=3).

Based on these examinations, it is concluded that high aspect ratio device does not have remarkable advantage than low aspect ratio device, and the latter device has similar capability for the prospect of future commercial reactor to the former device.

Keywords : Tokamak Reactor, ITER, Conceptual Design, System Analysis, Aspect Ratio, Steady State Operation, Divertor

JAERI-M 92-136

ITER（国際熱核融合実験炉）の設計オプションに関する低アスペクト比炉と高アスペクト比炉の比較研究

日本原子力研究所那珂研究所ITER開発室
杉原　正芳・多田　栄介・下村　安夫・常松　俊秀
西尾　　敏・仲里　敏子*・村上　好樹*・小泉　興一
ITER設計チーム

（1992年7月1日受理）

ITERの設計オプションとして，低アスペクト比炉と高アスペクト比炉の長所及び短所を定量的に比較研究した。ITERパワー則を仮定し，同じ自己点火能力を有するアスペクト比（A）3と4の炉を研究対象とした。アスペクト比4の炉における定常運転性能の改善は小さい。たとえば，アスペクト比を3から4に増加したことによって，Q値は約1増大し，ブートストラップ電流は約10％増大するのみである。アスペクト比4の炉においては，垂直不安定性に対する安全マージンが低下するため，非円形度を約20％低下させ同じ安定化マージンを確保する必要がある。そのような低非円形度を採用すると，ダブルヌルダイバータではポロイダル磁場系のエネルギーが増大する。これを防ぐためには，シングル・ヌルダイバータを採用する必要がある。このようなA＝4の炉においては，A＝3の炉に比べてダイバータへの熱流束が増加することが詳細な二次元ダイバータ・コードによる解析によって示された。将来の商用炉においても，核融合出力を調整することによって，A＝3とA＝4とで定常運転に関してほぼ同様の性能の炉が期待できる。

工学に関する初期的な検討によれば，炉内構造物の保守的スペースは少なく，トロイダル磁石の重量及び超電導巻線がそれぞれ2倍になり，低アスペクト比炉に比べて高アスペクト比炉が必ずしも魅力的でないことが明らかになった。

以上の検討にもとずき，高アスペクト比炉が，低アスペクト比炉に比べて顕著な改善はないことが示された。また将来の商用炉においても低アスペクト比炉は，高アスペクト比炉と同様の性能を有することが明かとなった。

那珂研究所：〒311－01 茨城県那珂郡那珂町大字向山801－1

＊　㈱東芝より出向

Contents

目　　次

1. Introduction

The device parameters of ITER given by Conceptual Design Activities (CDA-ITER [1]) have been determined to achieve the required plasma performance of ITER, i.e., self-ignited burn, based on the two types of ITER L-mode energy confinement scaling laws, i.e., power-law and offset-linear law with reasonable fusion power of about 1 GW. If, however, one of these scaling laws is considered more reliable, different optimization can be made. In fact, if only the power law is considered, the product of aspect ratio and plasma current almost determines the plasma performance, so that choice of higher aspect ratio device with lower plasma current is also possible. Such choice may have its own merit due mainly to the reduced plasma current, which may mitigates the disruption effect and ease the steady state operation. However, several demerits should also be expected in such device, so that quantitative evaluation of these merits and demerits on the overall reactor system, i.e. plasma performance and engineering design, is of primary importance.

In this report, comparative study on the plasma performance and the engineering design of low and high aspect ratio devices for ITER design option is quantitatively examine. Device parameters of A=3 and 4 are chosen for the comparative study based on ITER power-law scaling to provide same ignition performance. Engineering design, though it is still primitive, is done to assess the critical issues such as coil systems, remote maintenance, disruption effect and so on.

In Chap. 2, physics assessments are done. First, the characteristics of steady state operation are examined by system code. Secondly, detailed study on the characteristics of vertical stability is performed to determine appropriate elongation for high A device. Then the detailed study on poloidal field system with regard to the choice of elongation is done. Choice of single null or double null divertor configuration is also discussed. Detailed 2D divertor code calculation is performed to compare the divertor peak heat load in low and high aspect ratio devices. Finally the experimental capability and reactor relevancy are compared for each device, mainly with regard to the steady state power reactor. In Chap. 3, the engineering features such as toroidal field magnet structure, overall machine configuration and maintenance scheme of in-vessel components are investigated and compared with the present ITER design. In Chap. 4, main conclusions are summarized.

2. Physics Assessment

2.1 Characteristics of Steady State Operation

1. Introduction

The device parameters of ITER given by Conceptual Design Activities (CDA-ITER [1]) have been determined to achieve the required plasma performance of ITER, i.e., self-ignited burn, based on the two types of ITER L-mode energy confinement scaling laws, i.e., power-law and offset-linear law with reasonable fusion power of about 1 GW. If, however, one of these scaling laws is considered more reliable, different optimization can be made. In fact, if only the power law is considered, the product of aspect ratio and plasma current almost determines the plasma performance, so that choice of higher aspect ratio device with lower plasma current is also possible. Such choice may have its own merit due mainly to the reduced plasma current, which may mitigates the disruption effect and ease the steady state operation. However, several demerits should also be expected in such device, so that quantitative evaluation of these merits and demerits on the overall reactor system, i.e. plasma performance and engineering design, is of primary importance.

In this report, comparative study on the plasma performance and the engineering design of low and high aspect ratio devices for ITER design option is quantitatively examine. Device parameters of A=3 and 4 are chosen for the comparative study based on ITER power-law scaling to provide same ignition performance. Engineering design, though it is still primitive, is done to assess the critical issues such as coil systems, remote maintenance, disruption effect and so on.

In Chap. 2, physics assessments are done. First, the characteristics of steady state operation are examined by system code. Secondly, detailed study on the characteristics of vertical stability is performed to determine appropriate elongation for high A device. Then the detailed study on poloidal field system with regard to the choice of elongation is done. Choice of single null or double null divertor configuration is also discussed. Detailed 2D divertor code calculation is performed to compare the divertor peak heat load in low and high aspect ratio devices. Finally the experimental capability and reactor relevancy are compared for each device, mainly with regard to the steady state power reactor. In Chap. 3, the engineering features such as toroidal field magnet structure, overall machine configuration and maintenance scheme of in-vessel components are investigated and compared with the present ITER design. In Chap. 4, main conclusions are summarized.

2. Physics Assessment

2.1 Characteristics of Steady State Operation

For the present comparative study, the device parameters of A=3, 4 and 5 are first determined to provide the same ignition performance based on the ITER-power confinement scaling law, which is considered most reliable from statistical view point. These are shown in Fig. 2.1, in which the contours of equi-enhancement factor for ITER-power law both for L- and H-mode (2.0 for L-mode and 0.72 for H-mode) are depicted on the plane of aspect ratio-plasma current (A-I_p plane). On the same plane, contours of equi-major radius are also shown by dotted lines. Plasma current can be further reduced when the device parameters are determined by H-mode scaling as shown in the figure, since the H-mode scaling has stronger major radius dependence. We can choose three representative option devices 1, 2 and 3 on the figure. The device 1 is very similar to the CDA ITER, which represents low aspect ratio device, and the device 2 is a typical high aspect ratio device. We will call the former device as ITER-like and the second ITER-A. These two devices are mainly used for the present comparative study. In this calculation, we have assumed that the maximum toroidal field is 13.5 T, neutron wall loading is 1 MW/m^2 and the elongation is 1.9. The elongation κ is slightly reduced from the ITER value of κ=2, since it is anticipated that the plasma is less stable for vertical instability when the aspect ratio is increased. Actually, as shown in the next section, reduction of κ down to 1.9 is insufficient to attain the same stability margin for the present CDA ITER, while, in this study, we will employ κ=1.9 to draw the merit of high aspect ratio device. The device size is very sensitive to the value of κ and is shown in Table 2.1. In the LLNL study [1], the device size is considerably small (i.e., major radius is 6 m). This discrepancy is well explained by the difference of elongation κ and triangularity δ as shown in Fig. 2.2. Differences of 0.1 in κ and 0.05 in δ result in difference of 0.6 m in major radius. In ITER-A, δ is reduced to maintain the same divertor space as CDA ITER as shown later.

Plasma performance in the steady state operation for these option devices are now examined. Although the confinement performance is insensitive to fusion power or wall loading. In the case of power law, divertor performance is sensitive. A certain wall load is required blanket test which will be dome around midplane of outboard. Thus, peaking factor of wall loading is important. We compare the peaking factor of INTOR (A=4.4) and CDA ITER (A=2.8). In INTOR, the peaking factor P_f is 1.3 [2] and in CDA ITER, P_f is 1.6. Based on these values, P_f=1.6 for A=3 and P_f=1.37 for A=4 are employed. Figure 2.3 shows the operation region of steady state plasma on the plane of plasma temperature and plasma current (T-I_p) for ITER-like (a) and ITER-A (b) devices. On the plane, contours of equi-enhancement factor (H=2.1; solid line), Troyon coefficient (G=3; dash-dotted line) and current drive power (120MW; dotted line) and equi-Q (Q=5; long dotted line) are depicted. The region encircled by the contours of equi-H, 120MW of current drive power and

the limiting line of q_ψ=3 (horizontal dotted line) is allowed for steady state operation. Within this operation region, we will examine the plasma performance for two representative operation points. One is the maximum Q operation point with highest plasma current (A) and the other is the maximum bootstrap fraction operation point with lowest plasma current (B). In the former operation point (A), the required current drive power is smallest, which leads to the maximum Q value. In the latter operation point (B), both beta poloidal and q_ψ value are largest, which leads to the maximum bootstrap current fraction. In both of the operation points, it is seen that the available improvement of plasma performance is found only moderate i.e., Q and bootstrap fraction increase by about 1 and 10%, respectively, when A is increased from 3 to 4. Simple divertor model (H-K model [3] used in ITER) calculation shows the peak heat load per unit area on divertor plate decreases very moderately, i.e. only about 10%, with increasing A from 3 to 4, when double null divertor configuration is employed for both of the devices. Results of the more detailed 2D divertor code calculation is shown in the later section.

Figures 2.4 and 2.5 show the available Q-value (a), bootstrap current fraction (b) and peak heat load on divertor evaluated by simple model (c) in the operation point (A) and (B), respectively, for the device with aspect ratio of A=3, 4 and 5. In these figures, evaluations are made for three different values of neutron wall loading at the testing region (a) and (b), while peak heat load on divertor is only evaluated for 1 MW/m^2 at the test region (c). More detailed system quantities for these operation points are summarized in Tables 2.2, 2.3 and 2.4 for A=3,4 and 5, respectively.

2.2 Characteristics of Vertical Stability

In this section, study of vertical stability characteristics for A=4 device is done within the framework of rigid model. Here, we will use the stability margin as a measure of vertical stability, which is defined as follows.

$$m_s = \frac{F_{stab.} - F_{destab.}}{F_{destab.}} \qquad (2\text{-}1)$$

where :

$F_{destab.}$ is the destabilizing vertical force acting on the plasma due to the curvature of the external equilibrium magnetic field.

$F_{stab.}$ is the stabilizing vertical force acting on the plasma due to the flux-conserving eddy currents flowing in the passive structure (i.e., as if it were ideally conducting).

Stability margin for vertical stability decreases by about 20% in A=4 device compared with A=3 device as shown in Fig. 2.6. Dominant reason for this reduction of stability margin is that the relative distance between the plasma surface and the stabilizing shell becomes larger compared with that between the plasma current center and the shell, since, in this calculation, the scrape off lager (SOL) thickness is kept constant for simplicity. Smaller stability margin results in larger increase of growth rate from the expected value due to the model uncertainties (e.g., plasma deformation, profile change). Disruption probability will be increased, since the power supply capability for the vertical position control will be exceeded in some occasions by this unpredicted increase of growth rate.

Plasma elongation κ must be decreased from 2 down to about 1.8 in A=4 device to recover this reduction of stability margin as shown in Fig. 2.7. Increasing the triangularity δ could recover the stability margin to some extent, while full recover is not possible even when δ is increased up to 0.6. The effect of δ on the stability margin is shown in Fig. 2.8. Such large δ, e.g., 0.6, should cause the structural difficulty in the divertor region as shown later. In addition, plasma vertical position actually may become less stable due to the non-rigid effect of plasma motion.

2.3 Poloidal Field System

In the previous section, it is shown that the plasma elongation must be decreased by about 10 % in the higher aspect ratio device with A=4 due to less stability in vertical position. When this characteristics is taken into account in specifying the A=4 device, the choice of divertor configuration (single or double null) becomes fairly important, since the capacity of poloidal field system, which is well represented by its stored energy, is very sensitive to this choice. Figure 2.9 shows the required stored energy in poloidal field system vs plasma elongation for double (DN) and single (SN) null divertor configurations, respectively. As is seen from the figure, PF stored energy is very similar for DN and SN configuration when the elongation is large (e.g., $\kappa \approx 2.0$), while if DN configuration is employed for the smaller elongation (e.g., $\kappa \approx 1.8$), PF stored energy becomes enormously large. Single null divertor configuration should be employed for smaller elongation (≈ 1.8) to reduce the capacity of poloidal field system. Such large difference in stored energy between DN and SN configurations arises from the fact that generation of the null point with small elongation without placing PF coils at very near place to the null point require enormous PF current. In the case of SN configuration, elongation of the null point side can be larger than the non-null point side to attain the specified average elongation. In this calculation, the same coil location as CDA ITER is employed, while modification of the PF coil location (e.g., additional coil between PF5 and

PF6) will reduce this enormous increase to some extent.(not large). Vertical access scheme for the maintenance must be modified in this case. This feature has already been clarified in a previous study [4]. Increasing the triangularity δ also helps reducing the PF stored energy even when DN configuration is employed for smaller κ plasma. This feature is shown in Fig. 2.10, in which PF stored energy vs δ is shown for κ=1.83 and 1.75 in DN configuration. When δ is increased up to e.g., 0.6, the stored energy is decreased substantially, which is comparable to CDA ITER. In this case, however, the current of PF1 coil becomes significantly large to push the plasma inner surface as shown in Fig. 2.11. It is seen that the plasma almost starts to be indented, which requires large pusher-like coil current in PF1 coil. Available flux linkage will be lost significantly, which reduces the advantage of high A device in flux supply capability. Another deficit of large δ is that larger inboard space is necessary for installing divertor. This feature is shown in Fig. 2.12. It is seen from the figure that the major radius must be increased by more than 60 cm.

2.4 Divertor Performance

Detailed 2D divertor code (UEDA code [5]) calculations are done to evaluate the peak heat load per unit area on divertor plate in steady state operation for A=3 and A=4 devices. DN divertor configuration is assumed for A=3 device, while for A=4, both DN and SN configurations are examined. Operation point examined is the highest Q operation point. Details of the power flow balance to the divertor region for each operation point and divertor configuration are summarized in Table 2.5. Same perpendicular transport model in the SOL region as CDA ITER (i.e., $\chi_e = 2\,m^2/s$, $\chi_i = D = 2/3\,m^2/s$) is employed in the calculation. Overall geometry and mesh used in the calculation are shown in Fig. 2.13. Same divertor geometry i.e., distance from null to strike point (1.5m for outer and 0.6m for inner), angle of plate inclination (15° for outer and 45° for inner), is employed for all of the calculations, which is shown in Fig. 2.14.

Figure 2.15 shows the calculated peak heat load on the outer divertor plate of DN divertor configuration for A=3 and 4 devices. Dotted line shows the peak load when the same average wall load is assumed for each device i.e., 0.62 MW/m^2. When the same wall load at the testing region (1 MW/m^2) is assumed for each device by considering the difference of peaking factor, peak load of A=4 device becomes larger as shown by solid line. It is seen that the peak heat load per unit area of A=4 device decreases by 20-30% from that of A=3 device. Next we will evaluate the peak heat load in the case of SN divertor configuration for A=4 device. In this calculation, asymmetry of power onto the inner and outer divertor must be considered. Figure 2.16 shows the peak heat load

evaluated by UEDA code for inner (closed circle) and outer (open circle) divertor plate vs the fractional power to the outer divertor for the average wall load of 0.62 MW/m^2. Most of the experiments show that the asymmetry depends on the direction of toroidal field, and it is more pronounced when the ∇B drift direction is toward the null point (+B) (typically $\approx$ twice of the power goes to the outer), and it is more equalized when the ∇B drift direction is away from the null point (-B). Thus, in the present calculation, we will assume that the fractional power to outer divertor is 0.7 for +B and 0.5 for -B direction. Consequently, the peak heat loads are $\approx$14 and $\approx$5 MW/m^2 in the case of +B direction for outer and inner divertor plate, respectively, and $\approx$6.5 and $\approx$15 MW/m^2 in the case of -B direction for outer and inner divertor plate, respectively. When the wall load of 1 MW/m^2 is assumed at the test region, these values are further increased.

Figure 2.17 shows the summarizing results of the calculation. Cross hatched lines for A=4 device show the peak heat load of inner and outer divertor plate in the case of SN divertor configuration. The highest and lowest value of these lines correspond to the wall load of 0.62 MW/m^2 for average and 1 MW/m^2 at the test region, respectively. Only divertor plate with higher heat load is shown for each toroidal field direction. In the case of DN configuration of A=3 device, the time averaged peak heat load, when vertically oscillated [6], is also shown by closed circle.

In conclusion, if DN configuration could be employed in A=4 device, the peak heat load per unit area of A=4 device decreases by 20-30% from that of A=3 device. However, if SN configuration should be employed in A=4 device, the peak heat load on either inner or outer divertor plate, depending on the ∇B drift direction, increase on the contrary compared with A=3 device with DN configuration. In addition, the peak heat load of A=3 with DN configuration can further be reduced by employing vertical oscillation to produce alternate SN configuration. Comparison of these results show that the peak heat load of A=4 with SN configuration is 30-40% larger than that of A=3 with DN configuration.

2.5 Experimental Capability and Reactor Relevancy

Large experimental capability to obtain the data base for demo-reactor is very important for ITER. Although the concept of demo-reactor has not been fully identified yet, efficient steady state operation with high Q and high bootstrap fraction will be one of the most credible candidate operation scenarios as demonstrated by the reactor studies of SSTR [7] and ARIES-I [8]. Thus, in this section, we will examine and compare the experimental capability and reactor relevancy both for A=3 and 4 devices with particular emphasis on the steady state operation.

Let us first examine the experimental capability in achieving the steady state operation with high Q and high bootstrap current fraction. For this purpose, it is convenient to rewrite the Q value and bootstrap current fraction in the following way.

$$Q = \frac{P_f}{P_{in}} \propto \frac{5}{\dfrac{c(1+1.5f_{He}+3.5f_c)^2}{(AI_p)^2H^2} + \dfrac{2P_{rad}}{P_\alpha} - 1} \qquad (2\text{-}2)$$

$$\frac{I_{bs}}{I_p} \propto (q\sqrt{A}G)^{1.3} \qquad (2\text{-}3)$$

Here, f_{He}, f_c, P_{rad}, P_α, q and c are helium and carbon concentration, radiation power loss, α-particle heating power, safety factor and numerical constant, respectively. It is seen from these equations that Q value should basically be similar for A=3 and 4 devices, since the value of AIp is almost same for these devices to provide same ignition capability. Very moderate improvement obtained in Q value as shown Fig.2.3 arises from the fact that the operation density becomes slightly higher in A=4 than A=3 device due to the reduced necessary driven current in the former device. This increase of the operation density results in lower concentration of carbon and lower radiation power fraction, which leads to slightly higher Q value. On the other hand, the bootstrap fraction should be improved following Eq. (2-3), while the improvement is very moderate due to the weak dependence on A ($A^{0.65}$). Consequently, in either A=3 and 4 devices, experiment of steady state operation with simultaneous achievement of significantly high Q and high bootstrap current fraction will be difficult, when the plasma performance is followed by the reference physics guideline of ITER, i.e., G≤3, H≤2 and 10% of helium concentration.

Let us now examine the steady state performance, when the extended plasma performance could be realized. We assume G=3.5, H=2.3 and 5% of helium concentration in this study. Table 2.6 shows the calculation results. It is seen from this table that the experimental capability of steady state operation with significantly high Q and high bootstrap fraction can be expected even in A=3 device (Q more than 10 with bootstrap fraction of 30-50% is possible), comparable to that of A=4 device. If we further assume that the central q value (q_0) can be maintained about 2, still higher bootstrap fraction (more than 70% in A=3 device) can be expected as shown in the table. This maintenance of q_0 value will be reasonably expected, since, in this experiment, the plasma current is reduced and the edge q value is resultantly increased. In

conclusion, there will be no essential difference in the experimental capability of steady state operation between A=3 and 4 devices.

Next, we will actually demonstrate that high efficient steady state reactor with high Q and high bootstrap current fraction can be realized even in low aspect ratio reactor (called ITER-SSTR hereafter). For this study, it is convenient to further rewrite Eqs (2-2) and (2-3) as follows.

$$\frac{I_{bs}}{I_p} \propto (q\sqrt{A}G)^{1.3} \propto (AP_f^{0.5})^{1.3} \tag{2-4}$$

$$Q \propto \frac{GaB\kappa}{1 - c(AP_f^{0.5})^{1.3}} \tag{2-5}$$

It is understood from these equations that the key points for high Q and high bootstrap fraction are (i) high q and/or (ii) high fusion power. In fact, the last relation of Eq. (2-4) shows that the same bootstrap fraction can be realized even in ITER-SSTR by increasing the fusion power up to 4 GW as that of SSTR with the fusion power of 3 GW (A=4). In addition, if we assume the same technical bases as SSTR, i.e., maximum toroidal field B_{max}=16.5 T, current density j=365 A/mm^2 and the TF coil stress can be increased 1.3 times of ITER, low A reactor with very similar size to ITER can be designed. Comparison of major parameters between SSTR and ITER-SSTR are summarized in Table 2.7. More detailed parameters and radial build of ITER-SSTR are shown in Table 2.8 and Fig. 2.18, respectively.

Table 2.1 Major device parameters of A=4 device for different choice of elongation κ(κ=1.8 and 1.9) and confinement scaling laws (ITER power L-and H-mode).

	$2\tau_E$(L-mode)		$0.72\tau_E$(H-mode)
κ	1.8	1.9	1.9
R(m)	7.2	6.6	6.2
a(m)	1.8	1.65	1.55
I_p(MA)	15	15	13.8
P_w(MW/m^2)	1	1	1

Table 2.2 Detailed system parameters of A=3 device for the typical operation points (maximum Q and maximum bootstrap fraction) with different wall loading conditions.

P_w (MW/m²)	0.63		0.5		0.75	
Operation point	(A)	(B)	(A)	(B)	(A)	(B)
1						
2 Plasma Major Radius	5.7	5.7	5.7	5.7	5.7	5.7
3 Plasma Minor Radius	1.9	1.9	1.9	1.9	1.9	1.9
4 Plasma Current	20.0539	14.0009	20.0539	14.8	20.0539	12.9995
5 Bootstrap Current	4.2728	4.3706	3.8246	3.9515	4.6662	4.804
6 NB Driven Current	15.7811	9.6303	16.2293	10.8485	15.3877	8.1955
7 Safety Factor	3	4.297	3	4.065	3	4.628
8 Ope. Temp. (Den. Weighted)	23	15	23	16.5	23	13
9 Electron Density (x10^20)	0.6265	0.7729	0.5713	0.6641	0.6746	0.934
10 Ion Density (x10^20)	0.4961	0.6298	0.444	0.5309	0.5406	0.7728
11 DT Fuel Density (x10^20)	0.4218	0.5409	0.3749	0.4529	0.4615	0.6672
12 Total Beta	3.5952	2.7955	3.2296	2.6479	3.9092	2.8843
13 Fast Alpha Beta	0.6408	0.388	0.5577	0.3919	0.7114	0.3455
14 Beam Beta	0.6527	0.3983	0.6712	0.4487	0.6364	0.339
15 Poloidal Beta	0.6374	0.9831	0.5853	0.8531	0.6821	1.151
16 Troyon Coeff. (exc. beam pr	2.0206	2.2504	1.8151	2.0165	2.1971	2.5008
17 Troyon Coeff. (inc. beam pre	2.3875	2.5711	2.1924	2.3582	2.5548	2.7947
18 Average Zeff	2.1856	1.9239	2.3499	2.0993	2.0781	1.7785
19 DT Fraction	0.6732	0.6998	0.6562	0.682	0.6842	0.7143
20 Helium Fraction (given)	0.1	0.1	0.1	0.1	0.1	0.1
21 Carbon Fraction	0.017	0.0136	0.0192	0.0159	0.0156	0.0118
22 Oxygen Fraction (given)	0.001	0.001	0.001	0.001	0.001	0.001
23 Iron Fraction	0.0006	0.0004	0.0008	0.0006	0.0005	0.0003
24 DT Fuel Den./Ele. Den.	0.7918	0.8149	0.7772	0.7995	0.8014	0.8274
25 Fusion Power	590.1042	585.6626	466.186	469.5374	706.6333	711.4348
26 Alpha Power	118.15511	117.26576	93.34328	94.0143	141.48744	142.44885
27 NB Current Driven Power	111.197	118.621	105.3784	105.7912	116.0647	139.8783
28 Joule Power	1.1093	0.9037	1.1927	0.9551	1.0547	0.8926
29 Bremsstrahlung Power	5.6932	7.2738	4.6142	5.4885	6.7077	10.0934
30 Syncrotron Power (15%)	26.3711	10.7066	25.1819	12.4149	27.3634	8.4135
31 Wall Load at Plasma Surfac	0.6678	0.6628	0.5276	0.5313	0.7997	0.8051
32 Wall Load at First Wall	0.6256	0.6209	0.4942	0.4978	0.7492	0.7542
33 Voop Voltage	0	0	0	0	0	0
34 Q Value	5.3068	4.9373	4.4239	4.4383	6.0883	5.0861
35 Beam Energy (given)	1.3	1.3	1.3	1.3	1.3	1.3
36 NBCD Efficiency (Icd/Pnb)	0.1419	0.0812	0.154	0.1025	0.1326	0.0586
37 NBCD Figure of Merit	0.5068	0.3577	0.5015	0.3881	0.5098	0.3119
38 Radiation Power from Main	48.3324	36.7408	45.2764	34.7594	51.0985	40.5257
39 Radiation Power from Edge	17.2966	18.7121	16.8611	17.6273	17.7242	20.5809
40 Energy Confinement Time*	2.6195	1.9403	2.7947	2.1939	2.486	1.6852
41 H Factor for SO Scaling*	2.0865	1.6167	2.1561	1.7646	2.0269	1.4486
42 H Factor for Goldston*	1.8704	1.8637	1.9161	1.8571	1.8484	1.8894
43 H Factor for ITER-P*	2.0062	1.9866	2.0049	2.0006	2.0068	1.9691
44 H Factor for ITER-OL*	1.8097	1.6029	1.905	1.7393	1.7349	1.4611
45 H factor for Kaye-Big*	2.5291	2.3382	2.6149	2.3854	2.4809	2.3002
46 Wp	42.6093416	42.0955688	34.5290662	34.5920916	50.1877686	49.8801078
47 Tp	470.122127	303.584701	418.665588	310.641995	512.296853	264.914423
48 Ibs/Ip	0.21306579	0.31216565	0.19071602	0.26699324	0.23268292	0.36955268

Table 2.3 Detailed system parameters of A=4 device for the typical operation points (maximum Q and maximum bootstrap fraction) with different wall loading conditions.

	P_w (MW/m²)	0.74		0.6		0.88	
	Operation point	(A)	(B)	(A)	(B)	(A)	(B)
1	no.2						
2	Plasma Major Radius	6.6	6.6	6.6	6.6	6.6	6.6
3	Plasma Minor Radius	1.65	1.65	1.65	1.65	1.65	1.65
4	Plasma Current	15.3158	8.8022	15.3158	8.6497	15.3158	9.0005
5	Bootstrap Current	4.3038	4.71	3.8341	4.3096	4.7078	5.0561
6	NB Driven Current	11.0119	4.0922	11.4817	4.3401	10.608	3.9443
7	Safety Factor	3	5.22	3	5.312	3	5.105
8	Ope. Temp. (Den. Weighted)	22	10	21.5	10	22	10
9	Electron Density (x10^20)	0.7309	1.2595	0.6764	1.1455	0.789	1.3673
10	Ion Density (x10^20)	0.5919	1.0558	0.5423	0.9572	0.6442	1.1486
11	DT Fuel Density (x10^20)	0.5073	0.9154	0.4631	0.8291	0.5537	0.9966
12	Total Beta	2.6848	1.9064	2.4058	1.73	2.9195	2.0728
13	Fast Alpha Beta	0.4989	0.1674	0.4376	0.1506	0.5511	0.183
14	Beam Beta	0.3964	0.1473	0.4133	0.1562	0.3819	0.142
15	Poloidal Beta	0.9106	1.8375	0.8331	1.7477	0.9757	1.8953
16	Troyon Coeff. (exc. beam pre	2.1177	2.6165	1.8976	2.4162	2.3028	2.7821
17	Troyon Coeff. (inc. beam pre	2.4304	2.8187	2.2237	2.6344	2.6041	2.9727
18	Average Zeff	1.9811	1.6493	2.0744	1.6807	1.9047	1.6273
19	DT Fraction	0.6941	0.7268	0.6846	0.7238	0.7018	0.7289
20	Helium Fraction (given)	0.1	0.1	0.1	0.1	0.1	0.1
21	Carbon Fraction	0.0144	0.0103	0.0156	0.0107	0.0134	0.0101
22	Oxygen Fraction (given)	0.001	0.001	0.001	0.001	0.001	0.001
23	Iron Fraction	0.0005	0.0001	0.0005	0.0002	0.0004	0.0001
24	DT Fuel Den./Ele. Den.	0.8099	0.8382	0.8017	0.8356	0.8165	0.8401
25	Fusion Power	719.9558	721.8335	586.7158	592.1519	857.6609	855.573
26	Alpha Power	144.15497	144.53098	117.47665	118.56511	171.72731	171.30925
27	NB Current Driven Power	111.6302	150.4271	109.8781	144.6947	116.0026	157.7348
28	Joule Power	0.7362	0.6606	0.7979	0.6501	0.7078	0.6815
29	Bremsstrahlung Power	6.8662	14.3946	5.7346	11.8576	8.0897	17.0128
30	Syncrotron Power (15%)	37.9488	7.7171	34.5661	7.3596	39.428	8.0406
31	Wall Load at Plasma Surface	0.8102	0.8124	0.6603	0.6664	0.9652	0.9629
32	Wall Load at First Wall	0.7362	0.7382	0.6	0.6055	0.8771	0.8749
33	Voop Voltage	0	0	0	0	0	0
34	Q Value	6.4495	4.7986	5.3397	4.0924	7.3935	5.4241
35	Beam Energy (given)	1.3	1.3	1.3	1.3	1.3	1.3
36	NBCD Efficiency (Icd/Pnb)	0.0986	0.0272	0.1045	0.03	0.0914	0.025
37	NBCD Figure of Merit	0.4759	0.2261	0.4665	0.2268	0.4762	0.2257
38	Radiation Power from Main	60.5275	48.1357	55.1968	42.7221	64.1654	53.5821
39	Radiation Power from Edge	15.9571	21.8521	15.4927	20.4185	16.4921	23.272
40	Energy Confinement Time*	2.4055	1.5139	2.4565	1.5388	2.2763	1.4741
41	H Factor for SO Scaling*	2.4039	1.6121	2.3877	1.6187	2.3338	1.5882
42	H Factor for Goldston*	1.6662	1.8482	1.6137	1.8094	1.6615	1.8569
43	H Factor for ITER-P*	2.0293	2.0234	1.9663	1.994	2.0237	2.0235
44	H Factor for ITER-OL*	1.9814	1.6251	1.9986	1.6523	1.8968	1.5785
45	H factor for Kaye-Big*	2.8336	2.7395	2.7657	2.7004	2.8042	2.739
46	Wp	44.6505539	41.6264619	38.448999	37.3465645	52.6432742	46.6373634
47	Tp	339.614367	103.465398	320.273319	107.124463	368.734476	103.272466
48	lbs/Ip	0.28100393	0.5350935	0.25033625	0.49823693	0.30738192	0.56175768

Table 2.4 Detailed system parameters of A=5 device for the typical operation points (maximum Q and maximum bootstrap fraction) with different wall loading conditions.

	P_w (MW/m^2)	0.81		0.65		0.97	
	Operation point	(A)	(B)	(A)	(B)	(A)	(B)
1	no.3						
2	Plasma Major Radius	7.5	7.5	7.5	7.5	7.5	7.5
3	Plasma Minor Radius	1.5	1.5	1.5	1.5	1.5	1.5
4	Plasma Current	12.295	7.6004	12.295	7.4007	12.295	8.0011
5	Bootstrap Current	4.2979	4.6186	3.7931	4.2336	4.7906	4.8749
6	NB Driven Current	7.997	2.9819	8.5019	3.1671	7.5044	3.1262
7	Safety Factor	3	4.853	3	4.984	3	4.61
8	Ope. Temp. (Den. Weighted)	20	10	19.7	10	20.5	10
9	Electron Density (x10^20)	0.8363	1.3871	0.7637	1.256	0.8982	1.5145
10	Ion Density (x10^20)	0.6864	1.1657	0.6215	1.0528	0.7412	1.275
11	DT Fuel Density (x10^20)	0.591	1.0115	0.5335	0.9128	0.6394	1.1071
12	Total Beta	2.2503	1.673	2.0012	1.5121	2.4874	1.8291
13	Fast Alpha Beta	0.4308	0.1478	0.3708	0.1327	0.4795	0.1624
14	Beam Beta	0.2771	0.1033	0.2946	0.1097	0.26	0.1083
15	Poloidal Beta	1.2043	2.2148	1.0939	2.1329	1.3091	2.1798
16	Troyon Coeff. (exc. beam pr	2.2538	2.7106	2.0043	2.516	2.4913	2.815
17	Troyon Coeff. (inc. beam pre	2.5313	2.878	2.2993	2.6986	2.7517	2.9817
18	Average Zeff	1.8552	1.6238	1.9356	1.6501	1.8033	1.6053
19	DT Fraction	0.7067	0.7292	0.6987	0.7267	0.7118	0.731
20	Helium Fraction (given)	0.1	0.1	0.1	0.1	0.1	0.1
21	Carbon Fraction	0.0128	0.01	0.0138	0.0103	0.0121	0.0098
22	Oxygen Fraction (given)	0.001	0.001	0.001	0.001	0.001	0.001
23	Iron Fraction	0.0003	0.0001	0.0004	0.0001	0.0003	0.0001
24	DT Fuel Den./Ele. Den.	0.8208	0.8403	0.8138	0.8382	0.8253	0.8418
25	Fusion Power	836.0569	830.8894	670.2288	676.6077	1004.5498	995.2715
26	Alpha Power	167.40163	166.36693	134.19827	135.47546	201.13853	199.28073
27	NB Current Driven Power	117.4363	142.9266	115.1876	136.9955	116.2377	164.0169
28	Joule Power	0.4841	0.458	0.5166	0.4412	0.4534	0.5017
29	Bremsstrahlung Power	8.2274	16.5147	6.7312	13.4942	9.6779	19.735
30	Syncrotron Power (15%)	40.4086	10.014	37.2452	9.529	44.4214	10.4639
31	Wall Load at Plasma Surfac	0.9108	0.9052	0.7301	0.7371	1.0943	1.0842
32	Wall Load at First Wall	0.811	0.806	0.6502	0.6563	0.9745	0.9655
33	Voop Voltage	0	0	0	0	0	0
34	Q Value	7.1192	5.8134	5.8186	4.9389	8.6422	6.0681
35	Beam Energy (given)	1.3	1.3	1.3	1.3	1.3	1.3
36	NBCD Efficiency (Icd/Pnb)	0.0681	0.0209	0.0738	0.0231	0.0646	0.0191
37	NBCD Figure of Merit	0.4271	0.217	0.4227	0.2178	0.4349	0.2165
38	Radiation Power from Main	65.0271	53.7658	59.2211	47.3896	71.5307	60.3718
39	Radiation Power from Edge	15.9222	22.1072	15.2652	20.4803	16.5191	23.7641
40	Energy Confinement Time*	2.1081	1.52	2.1833	1.5607	2.08	1.4011
41	H Factor for SO Scaling*	2.4571	1.8352	2.465	1.8556	2.484	1.7313
42	H Factor for Goldston*	1.4548	1.6935	1.4139	1.6788	1.5129	1.6106
43	H Factor for ITER-P*	1.9272	2.0085	1.883	2.0026	1.9941	1.9085
44	H Factor for ITER-OL*	1.9686	1.7583	2.0088	1.8086	1.9651	1.6097
45	H factor for Kaye-Big*	2.9935	3.0821	2.9359	3.0737	3.0909	2.9281
46	Wp	48.5684449	40.4421571	41.0660614	35.5879938	55.1699334	49.8971154
47	Tp	271.916475	76.0929347	256.573913	77.3127066	282.802054	86.1719242
48	Ibs/Ip	0.34956486	0.60767854	0.30850752	0.57205399	0.38963806	0.60927872

Table 2.5 Power flow balance to the divertor region in A=3 and 4 devices for each divertor configuration. In A=4 device, power flow balance for two wall load conditions (0.62 and 0.74 MW/m^2) and divertor configurations (SN and DN) are shown.

	A=3	A=4	
Average wall load (MW/m^2)	0.62	0.62	0.74
a power (MW)	118	121	145
CD power (MW)	107	96	108
Power radiated (MW)	67	80	79
Power to SOL (MW)	158	137	174
Edge density ($10^{20}m^{-3}$)	0.18	0.19	0.21
Power fraction to one outer divertor plate (DN)	0.4	0.4	0.4
(SN)		0.44-0.65	

Table 2.6 Steady state performance, Q value and bootstrap current fraction (number shown in parenthesis) in extended plasma performance case (H=2.3, G=3.5 and f_{He}=5%) for CDA ITER and ITER-A (A=4) devices.

	CDA ITER	ITER-A
Maximum Q operation point	12 (0.31)	17.8 (0.45)
Maximum bootstrap fraction operation point*)	7.7 (0.54)	7 (0.78)
*) when control of $q_0 \approx 2$ is attained	≈10 (0.75)	≈10 (≈1.0)

Table 2.7 Parameters of low aspect ratio (A≈3) ITER-SSTR power reactor.

Assumption; same technical base for SSTR
- Bmax = 16.5 T
- j = 365 A/mm2
- TF coil stress; 1.3 times of ITER

	SSTR	ITER-SSTR
R (m)	7	~6.25
a (m)	1.75	~2.15
K	1.8	~2.0
I_p (MA)	12	~16.5
β_t	5	~5.7
I_b / I_p	0.75	~0.75
Q	50	~47
P_f (Mw)	3000	~3500
P_{CD} (Mw)	60	~75

Table 2.8 Detailed parameters of low aspect ratio (A≈3) ITER-SSTR power reactor

Plasma major radius (m)	6.25
Plasma minor radius (m)	2.15
Elongation	2
Triangularity	0.35
Plasma volume (m^3)	1118
Toroidal field (T)	7
Safety factor (95%)	5.51
Plasma current (MA)	16.5
Bootstrap current (MA)	11.24
Bootstrap fraction	68 %
NB driven current (MA)	5.26
Beta poloidal	1.91
Total beta (%)	4.6
Alpha beta (%)	0.99
Thermal beta (%)	3.49
Beam beta (%)	0.12
Troyon factor	4.2
Volume average temperature (keV)	15
Electron density ($10^{20}m^{-3}$)	1.25
Ion density ($10^{20}m^{-3}$)	1.11
Fuel density ($10^{20}m^{-3}$)	1.03
Zeff	1.55
DT fraction (%)	82.7
Helium fraction (%)	5
Carbon fraction (%)	1.03
Oxygen fraction (%)	0.1
Iron fraction (%)	0.013
Fusion power (MW)	4000
CD power (MW)	97.7
Fusion gain Q	40.9
Radiation from main (MW)	116
Radiation from main (MW)	36.5
Wall load at plasma surface (MW/m^2)	3.5
Wall load at first wall (MW/m^2)	3.36
Required confinement time (s)	1.46
H-factor for ITER89P/main	1.95
H-factor for ITER89OL/main	1.03

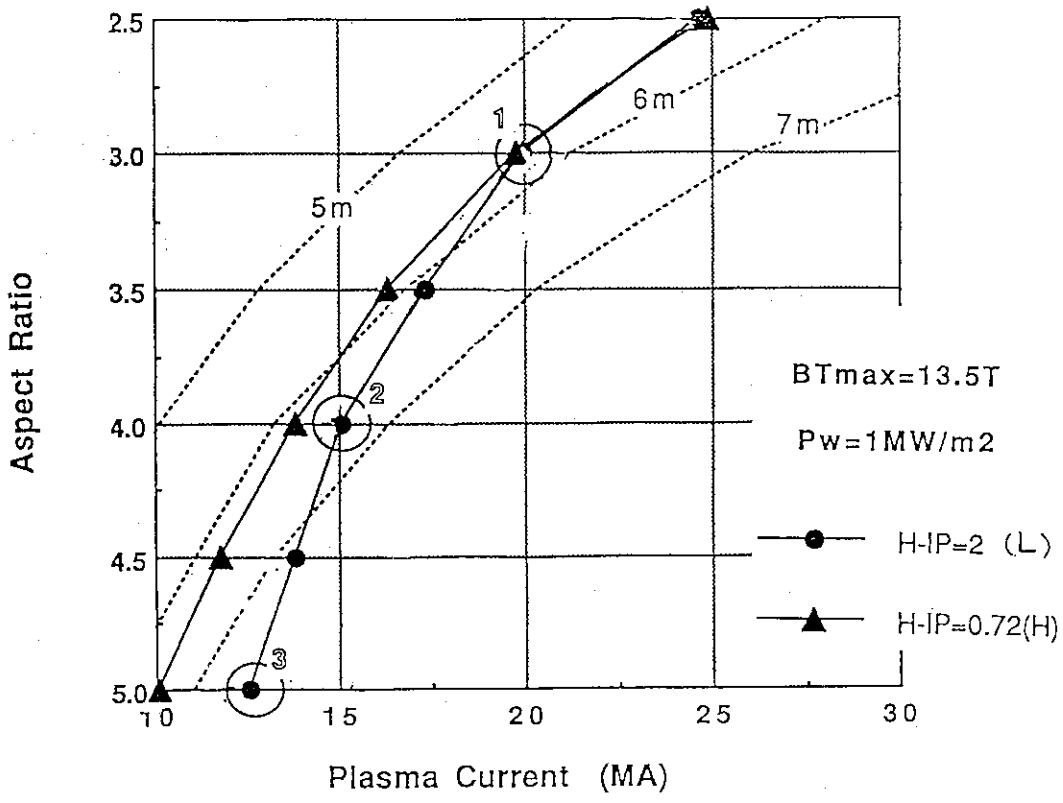

Fig. 2.1 Selection of device parameters for comparative study on A-Ip space. Device 1, 2 and 3 provide same ignition performance based on ITER power L-mode scaling (closed circles). Closed triangles denote the device parameters based on ITER power H-mode scaling law. Required major radii are indicated by dotted lines. B_{max}=13.5 T, κ=1.9 and P_w=1 MW/m^2 are assumed in the calculations.

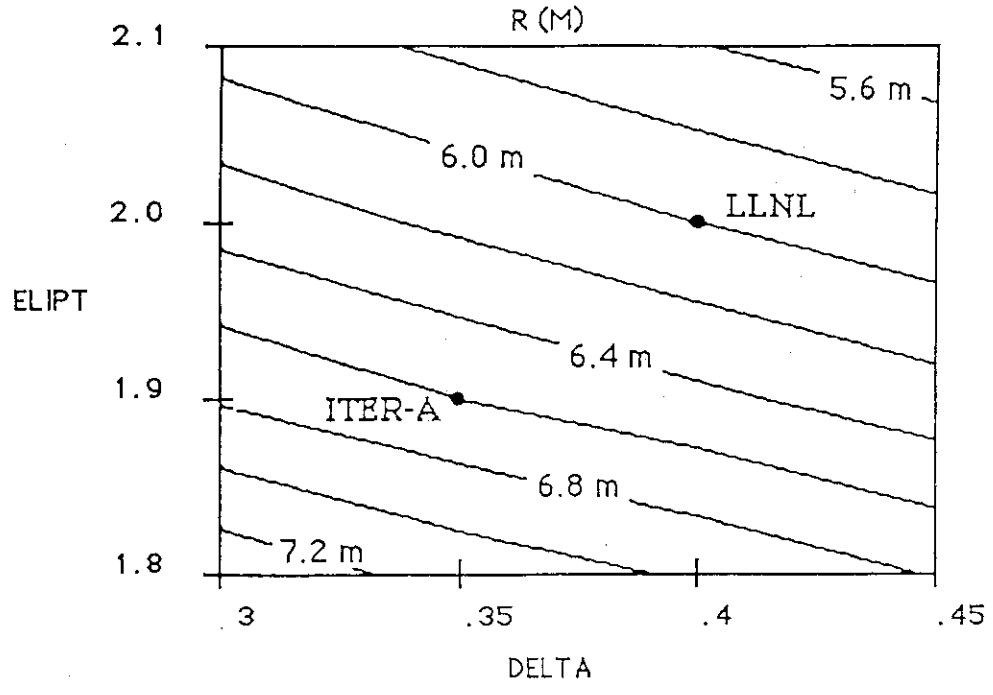

Fig. 2.2 Difference of the device parameters for A=4 device between ITER-A(JAERI) and LLNL's. Difference can be well explained by the difference of elongation and triangularity.

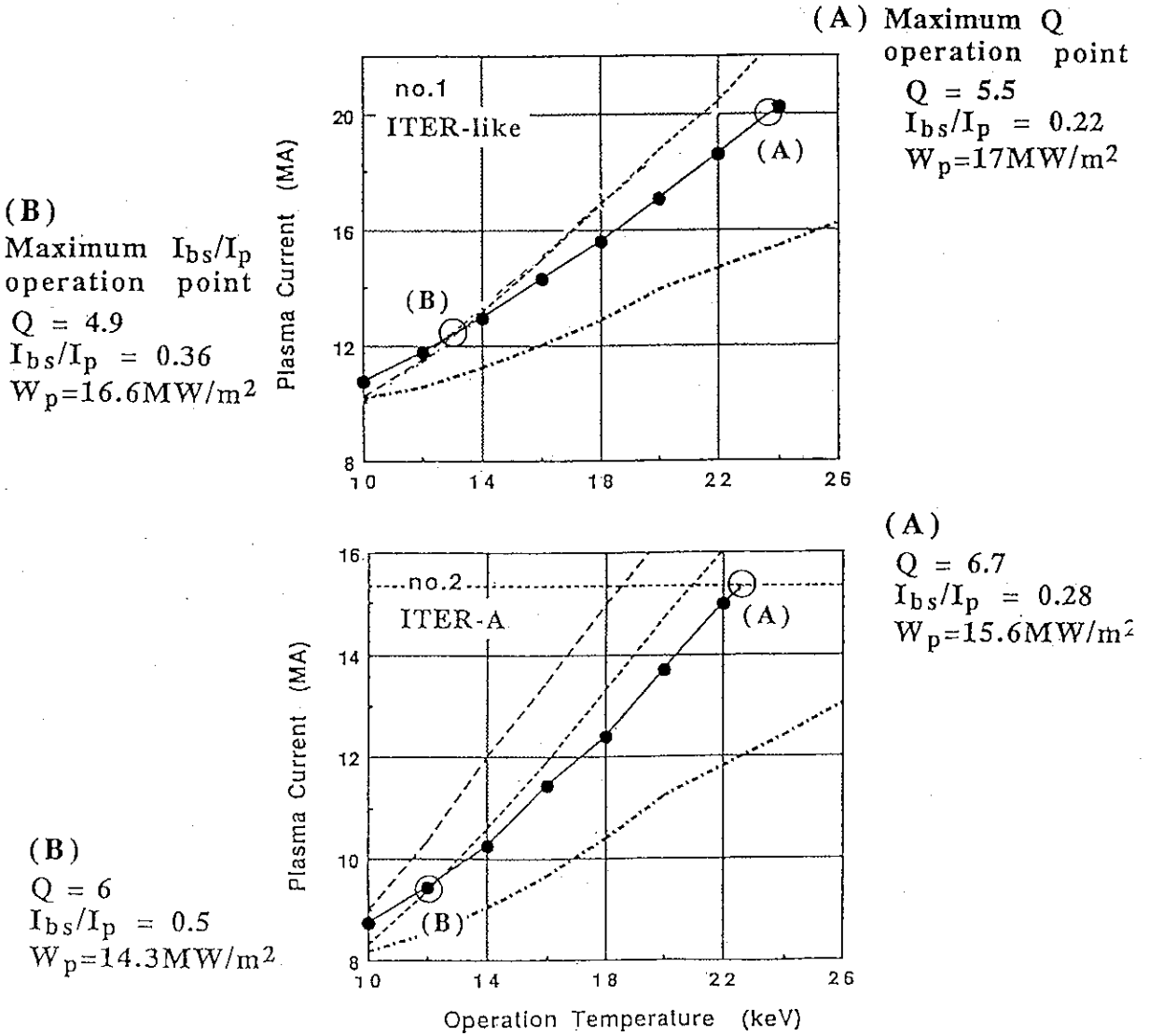

Fig. 2.3 Steady state operation region on the plane of plasma current and temperature, and the performances of typical operation points (maximum bootstrap fraction and maximum Q denoted as operation point (A) and (B), respectively) for ITER-like and ITER-A devices. Solid line, dash-dotted line, dotted line and long dotted line denote the limiting lines for confinement (H=2.1), beta (G=3), CD power (120 MW) and Q value (Q=5), respectively.

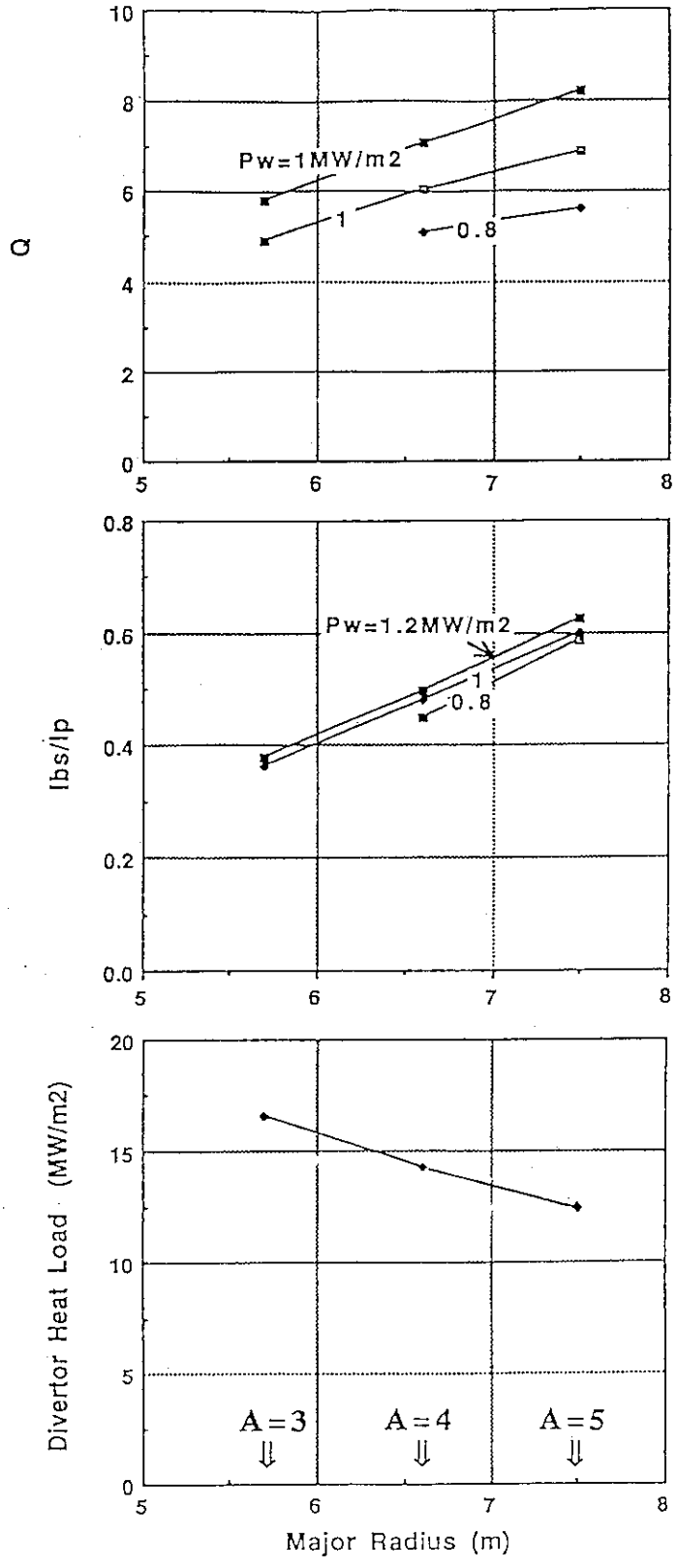

Fig. 2.4 Available Q-value (a), bootstrap current fraction (b) and peak heat load on divertor evaluated by simple model (c) at the operation point (A) for the device with aspect ratio of A=3, 4 and 5. Evaluations are made for three different values of neutron wall loading at the testing region (a) and (b), while peak heat load on divertor is only evaluated for 1 MW/m^2 at the test region (c).

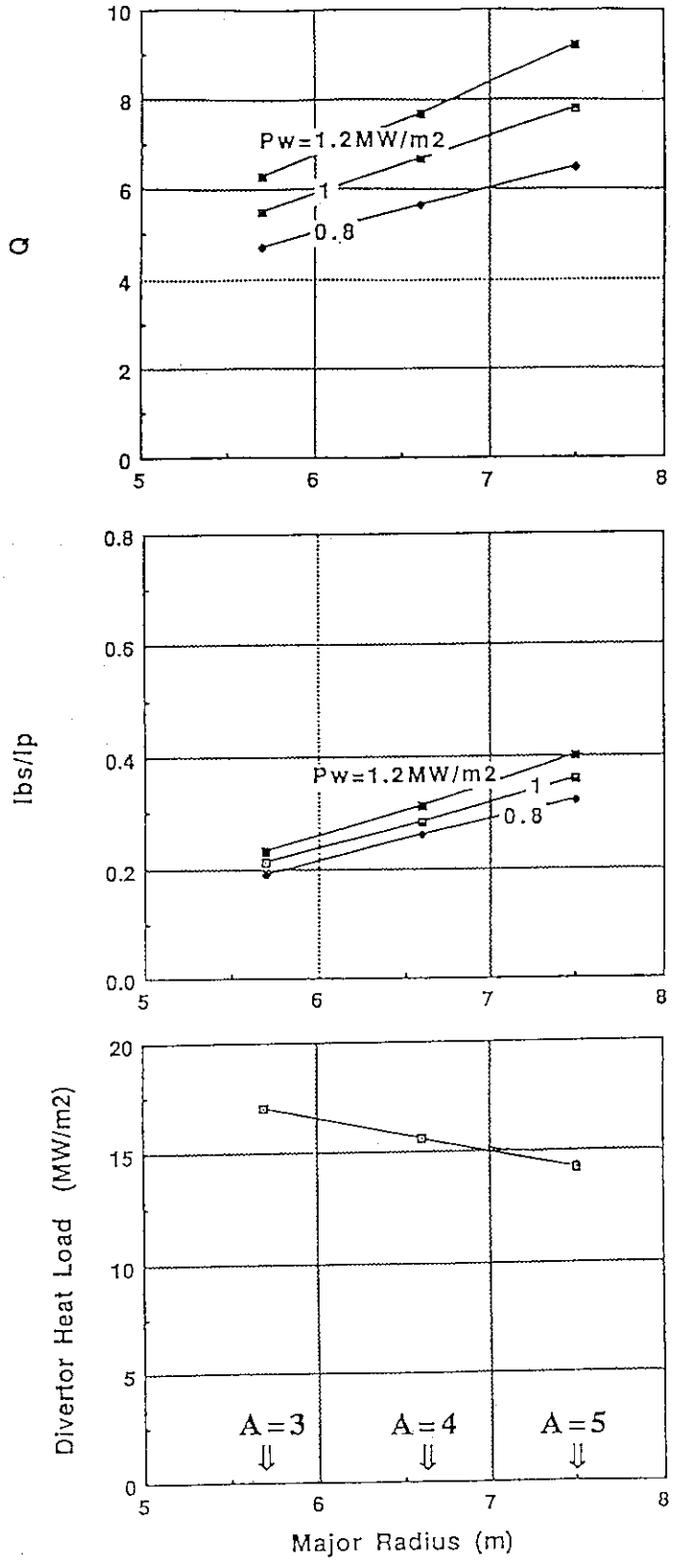

Fig. 2.5 Available Q-value (a), bootstrap current fraction (b) and peak heat load on divertor evaluated by simple model (c) at the operation point (B) for the device with aspect ratio of A=3, 4 and 5. Evaluations are made for three different values of neutron wall loading at the testing region (a) and (b), while peak heat load on divertor is only evaluated for 1 MW/m^2 at the test region (c).

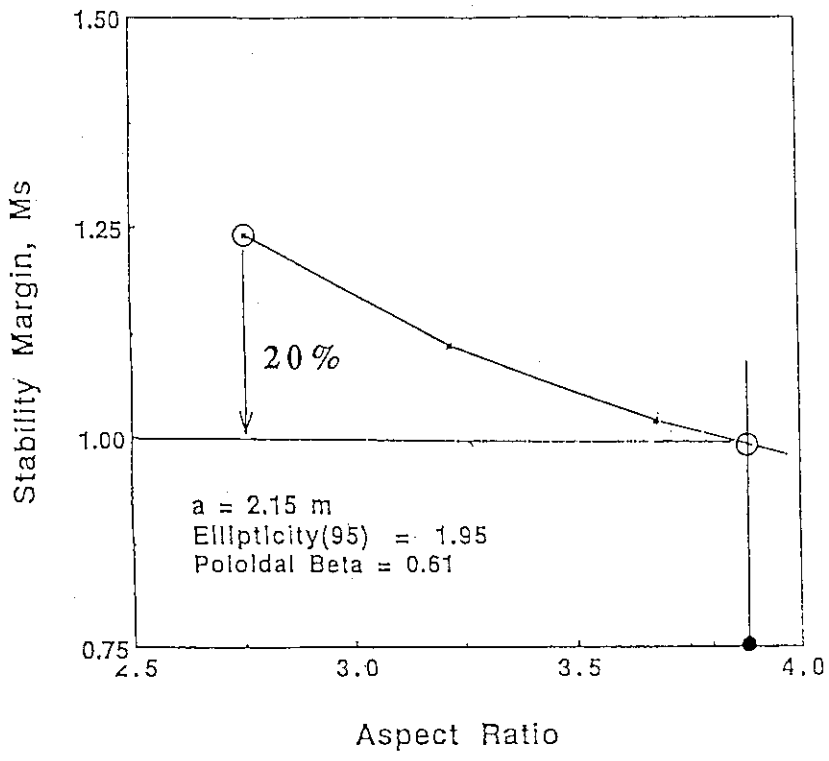

Fig. 2.6 Stability margin vs aspect ratio. Plasma size and relative distance between plasma surface and shell are kept constant in the calculation. Stability margin decreases by ≈ 20% when A is increased from ≈ 3 to ≈ 4.

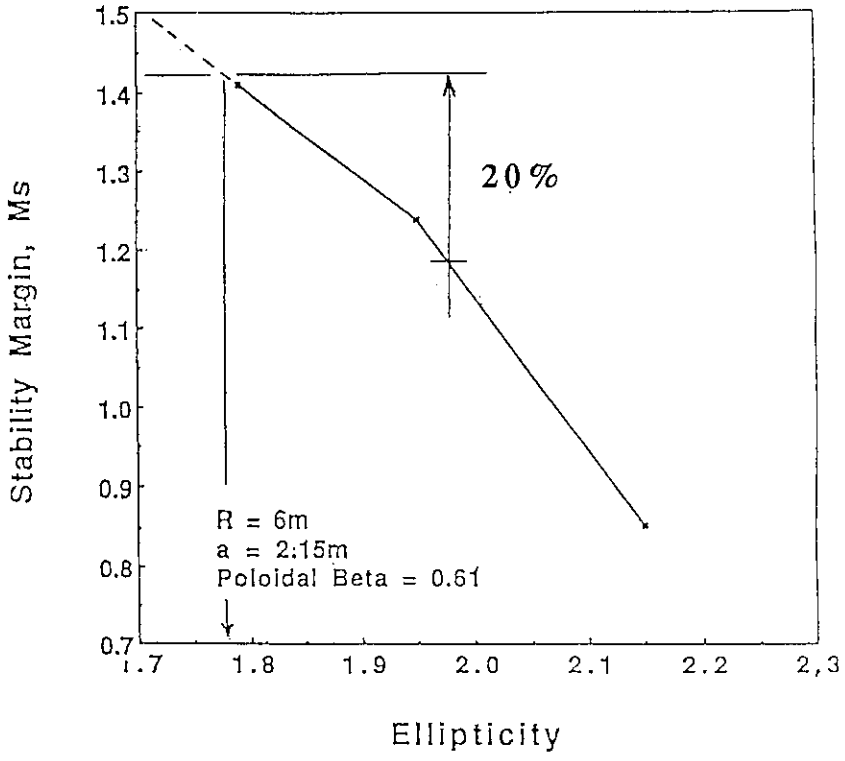

Fig. 2.7 Stability margin vs elongation. Plasma size and relative distance between plasma surface and shell are kept constant in the calculation. Elongation must be decreased by ≈ 10% to recover stability margin decreased by ≈ 20% when A is increased from ≈ 3 to ≈ 4.

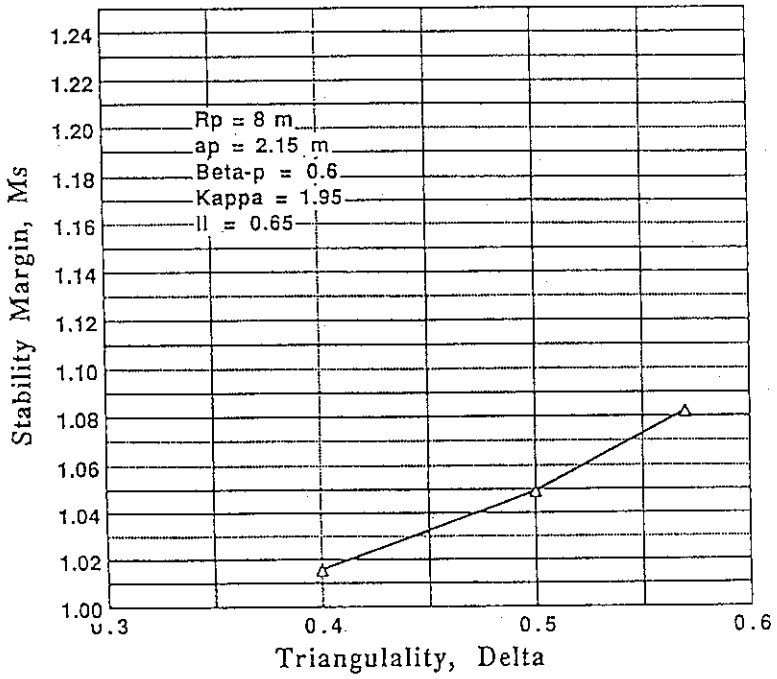

Fig. 2.8 Stability margin vs triangularity. Plasma size and relative distance between plasma surface and shell are kept constant in the calculation. Stability margin increases by≈10% when the triangularity increases from 0.4 to 0.6.

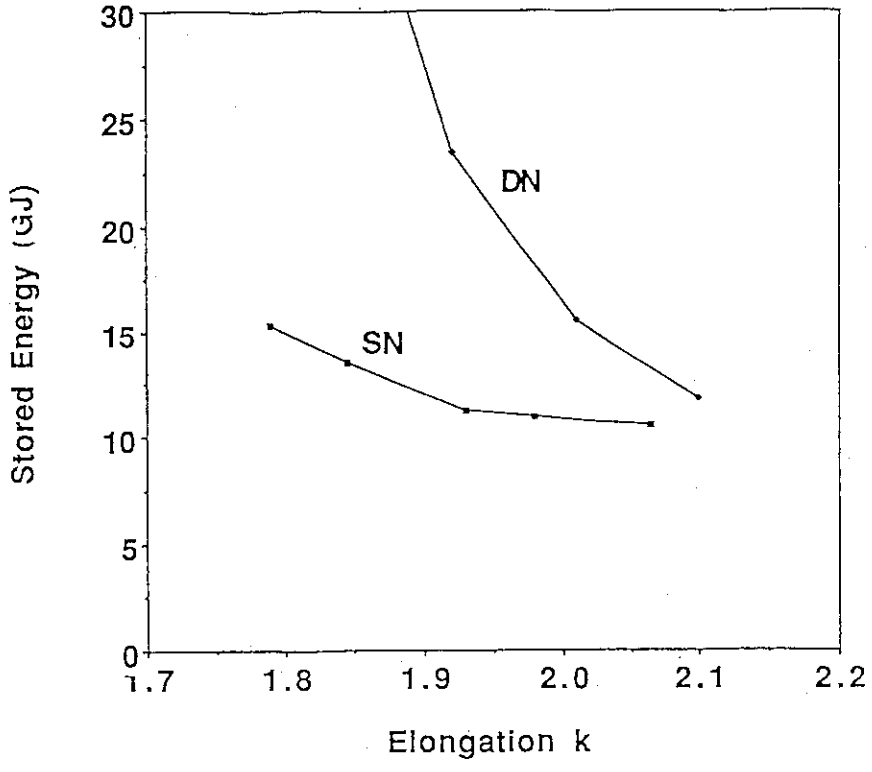

Fig. 2.9 Stored energy of poloidal field system vs elongation for double null (DN) and single null (SN) divertor configurations. Sharp increase of stored energy is expected for DN when elongation is decreased below 2. In SN case, energy increases only moderately unless elongation is decreased very below 2.

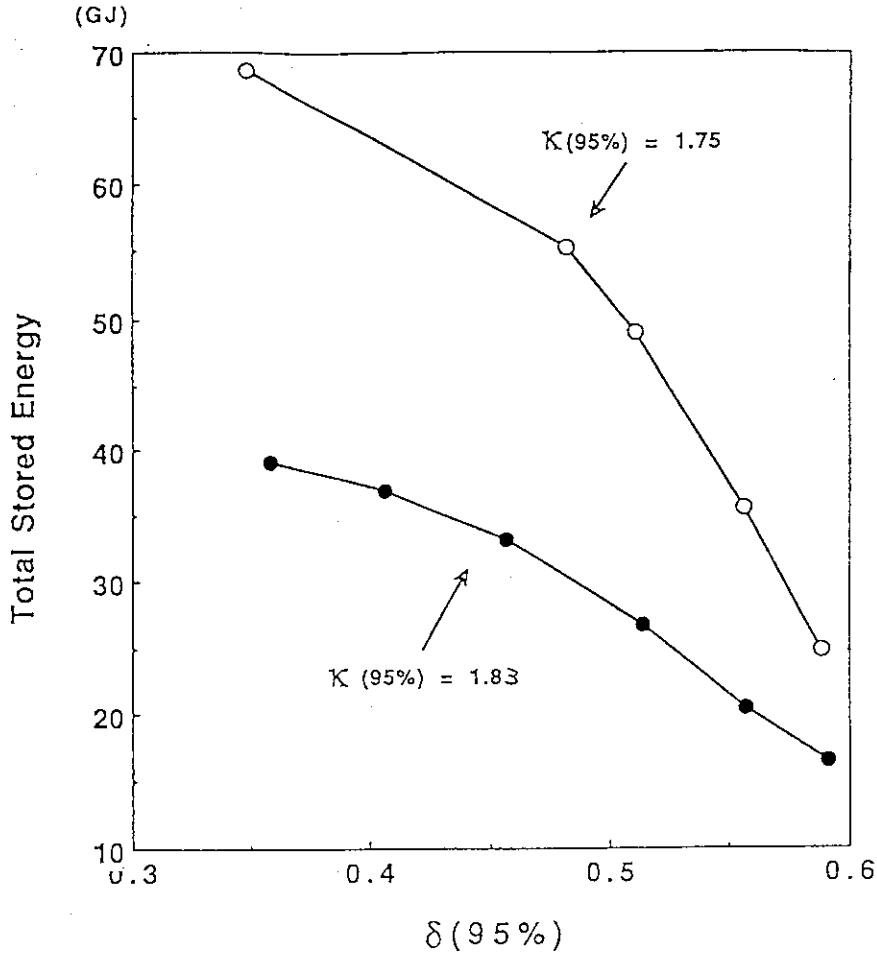

Fig. 2.10 Stored energy of poloidal field system vs triangularity for double null (DN) divertor configurations with κ=1.83 (closed circle) and 1.75 (open circle).

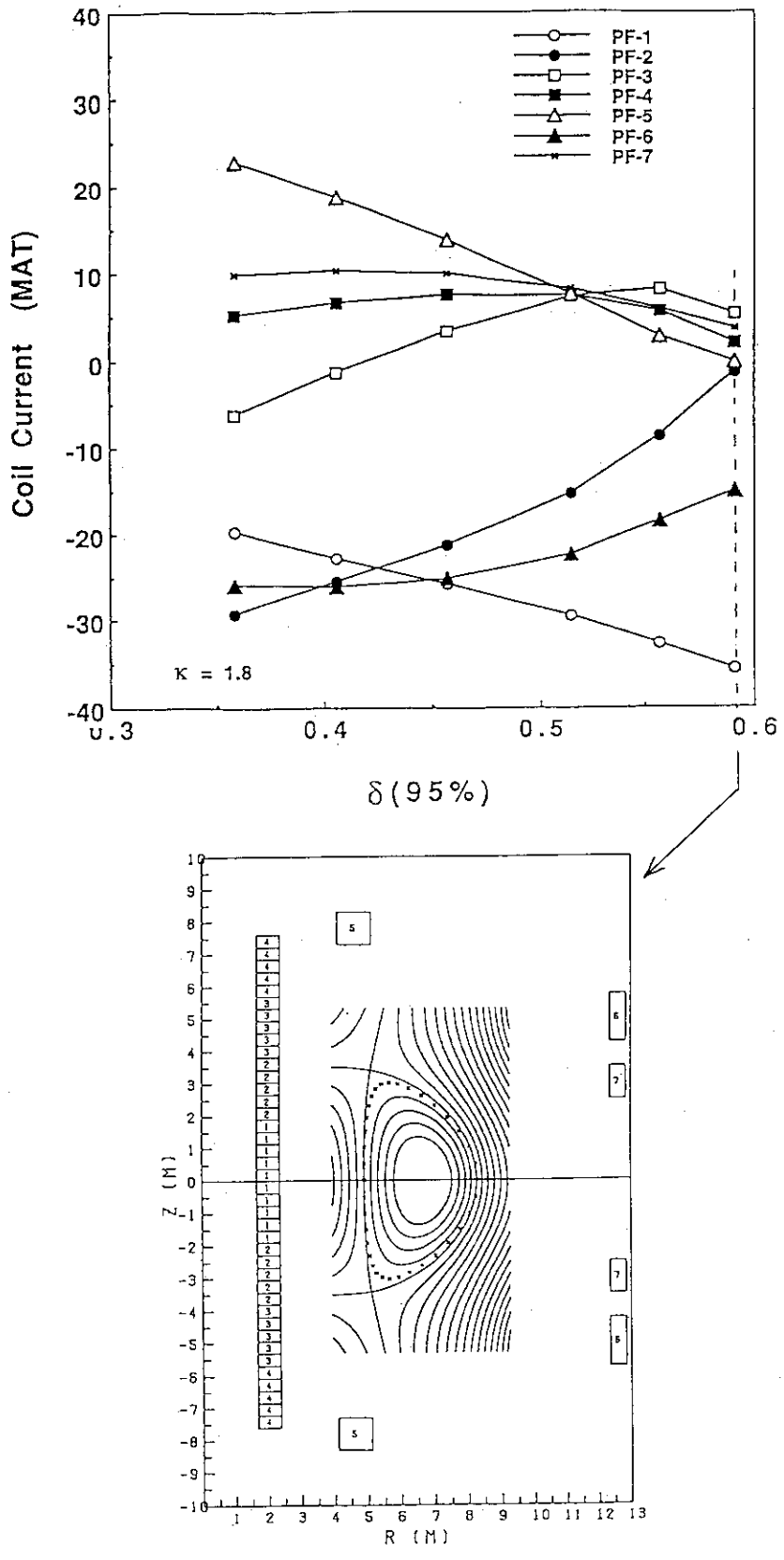

Fig. 2.11 PF coil current patterns vs triangularity for κ=1.8 with DN. When δ=0.6, PF1 coil current increases significantly.

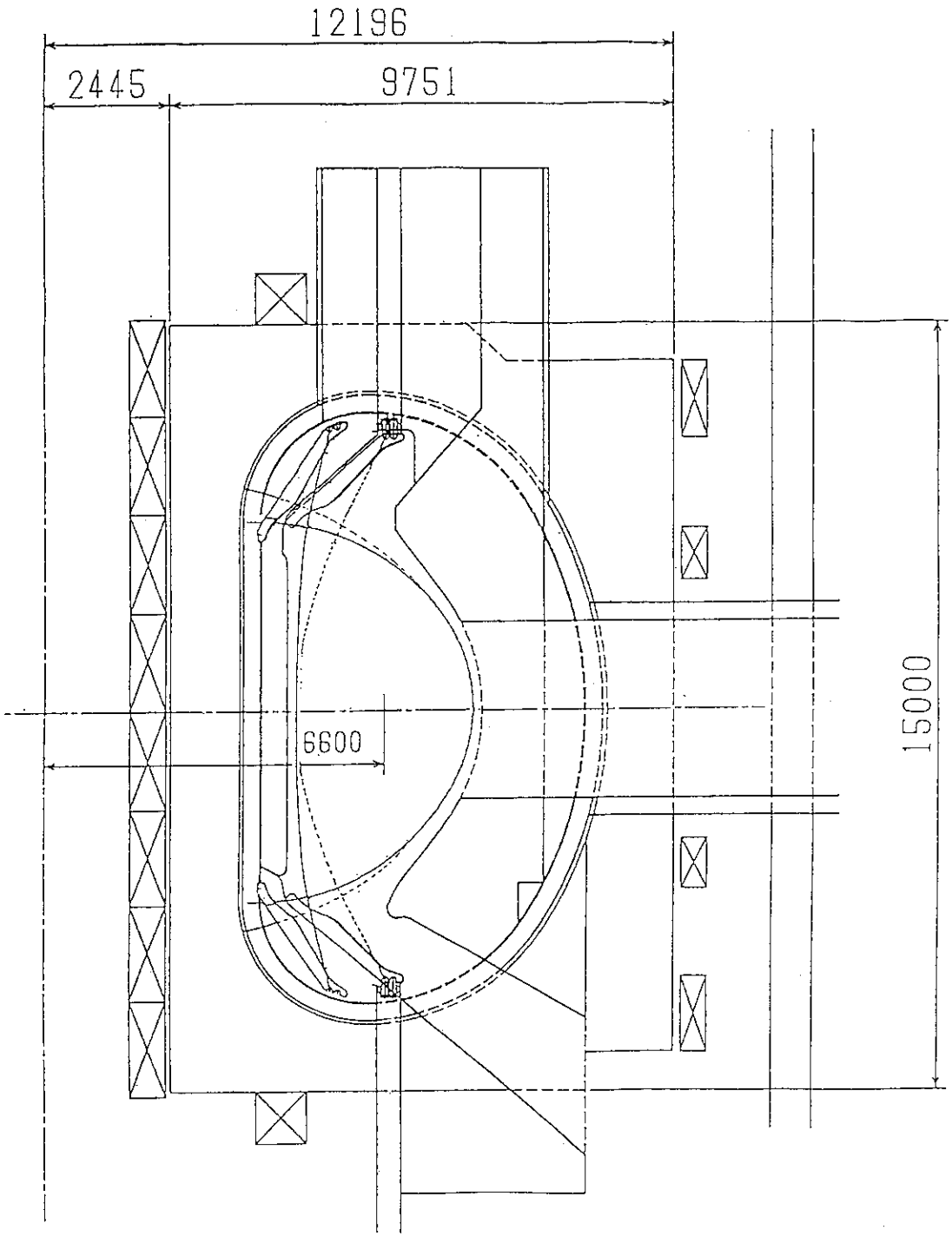

Fig. 2.12 Effect of high triangularity (δ=0.6) on divertor structure and inboard shield structure.

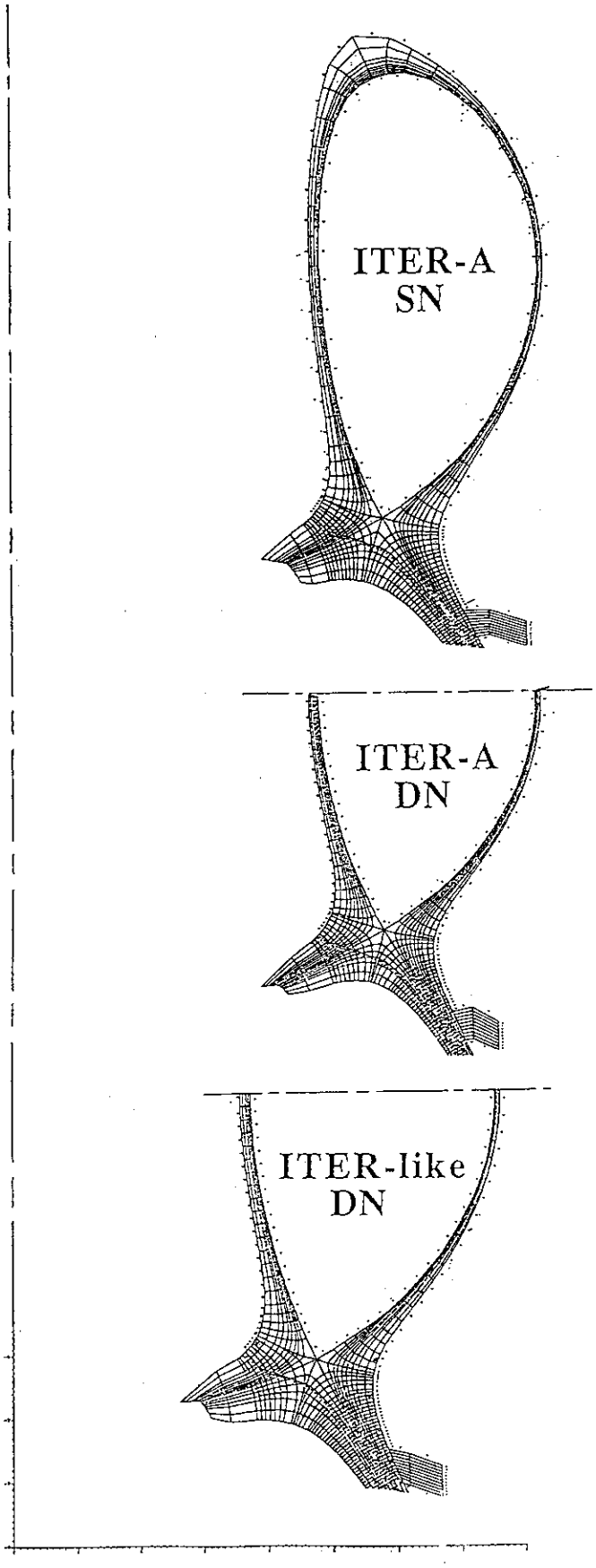

Fig. 2.13 Overall geometry and mesh used in the detailed 2D divertor code calculation. For A=4 device, both DN and SN configurations are examined.

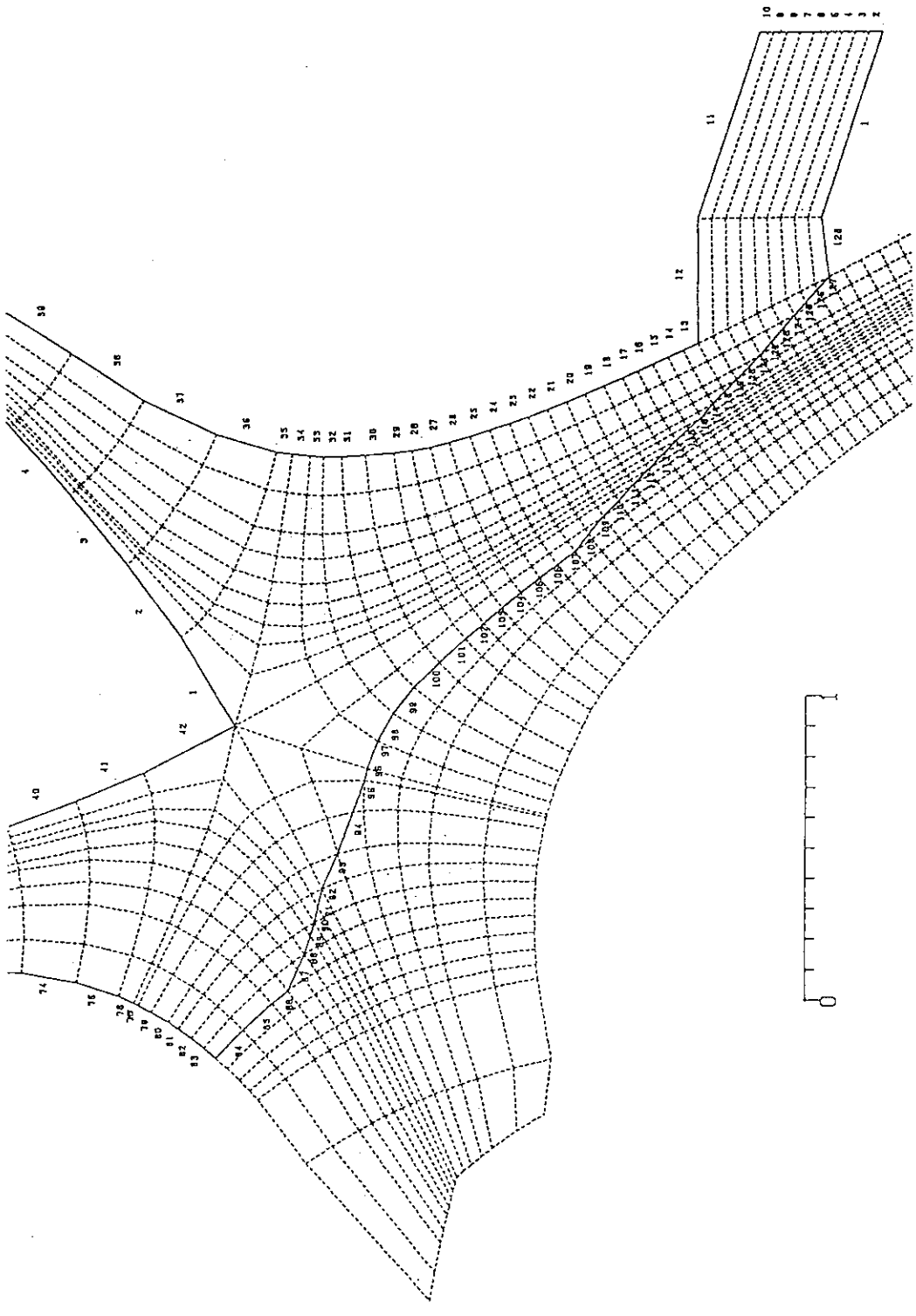

Fig. 2.14 Details of divertor geometry. Same distance from null to strike point (1.5m for outer and 0.6m for inner), angle of plate inclination (15° for outer and 45° for inner), is employed for all of the calculations

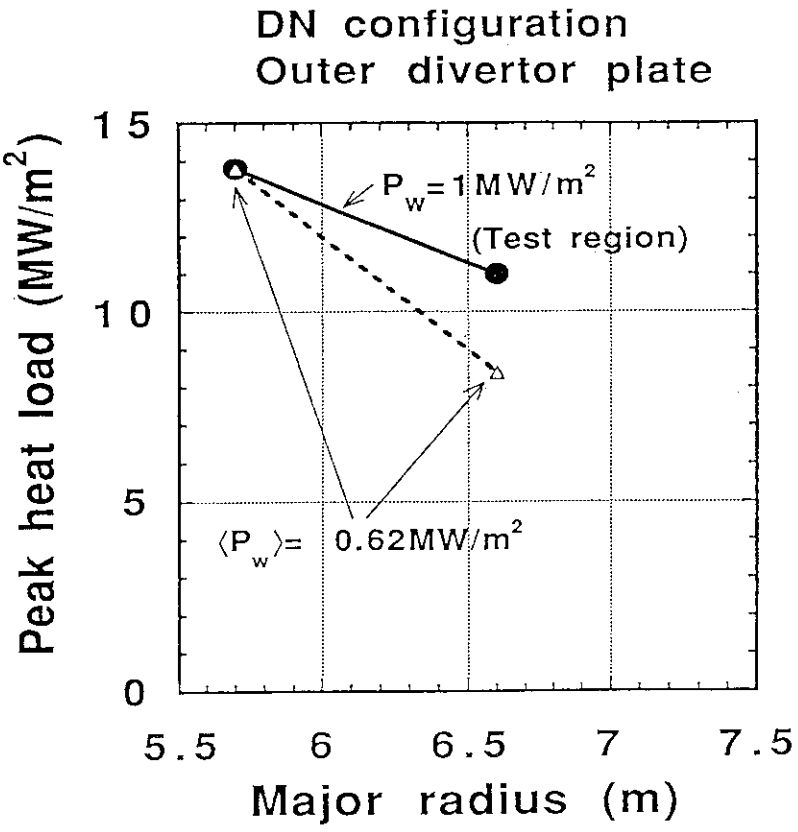

Fig. 2.15 Calculated peak heat load on the outer divertor plate of DN divertor configuration for A=3 and 4 devices. Dotted line shows the peak load when the same average wall load is assumed for each device i.e., 0.62 MW/m^2. When the same wall load at the testing region (1 MW/m^2) is assumed for each device by considering the difference of peaking factor, the peak heat load of A=4 device becomes higher as shown by solid line.

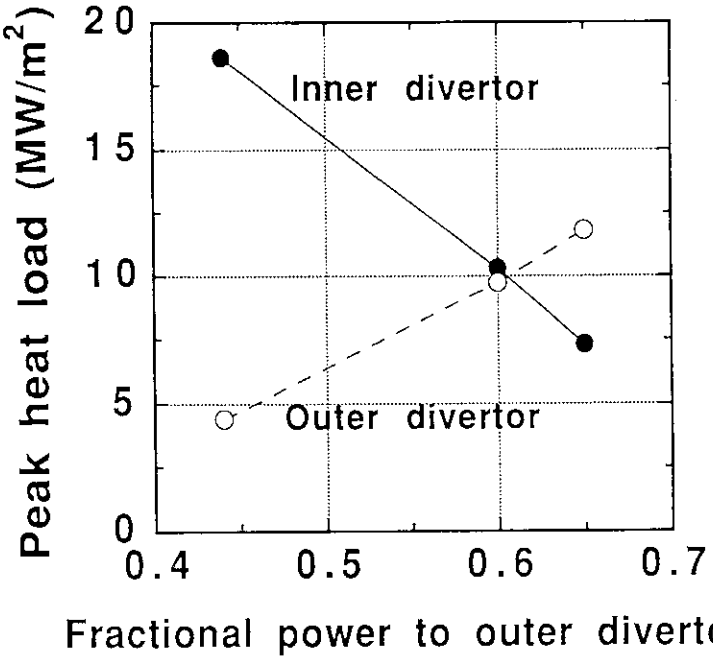

Fig. 2.16 Peak heat load on inner (closed circle) and outer (open circle) divertor plate in SN divertor configuration vs fractional power to outer divertor plate.

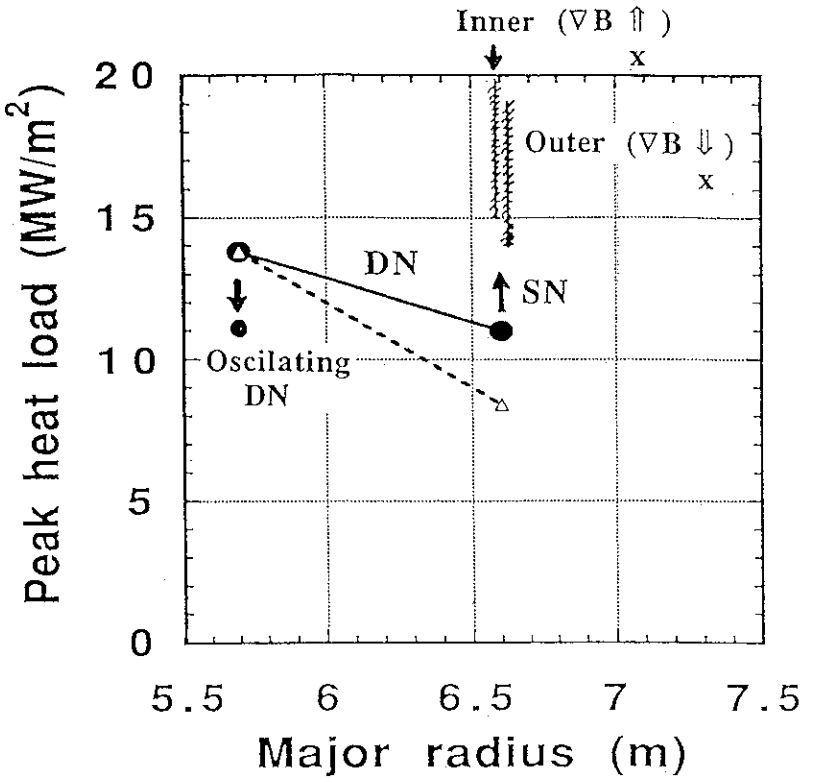

Fig. 2.17 Summary of peak heat load on divertor plate for A=3 and 4 devices. Cross hatched lines for A=4 device show the peak heat load of inner and outer divertor plate in the case of SN divertor configuration. The highest and lowest value of these lines correspond to the wall load of 0.62 MW/m^2 for average and 1 MW/m^2 at the test region, respectively. Only divertor plate with higher heat load is shown for each toroidal field direction. In the case of DN configuration of A=3 device, the time averaged peak heat load, when vertically oscillated, is also shown by closed circle.

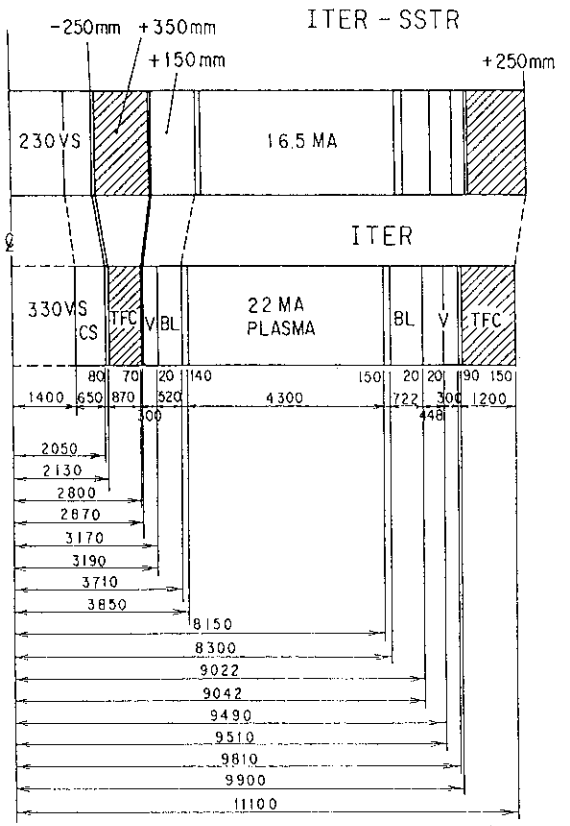

Fig. 2.18 Radial build of low aspect ratio steady state power reactor ITER-SSTR with comparison of CDA ITER.

3. Engineering Assessment

A high-aspect ratio reactor (high-A reactor) has been investigated and compared with the present ITER design (ITER-CDA) from viewpoint of engineering features. The major parameters of high-A reactor used in this comparative study are listed in Table 3.1.

Based on these parameters, the structural design of toroidal field magnet and maintenance scheme of in-vessel components were investigated and compared with the present ITER-CDA design.

3.1 Toroidal Field Magnet

The toroidal field (TF) magnet of high-A reactor concept is designed on the same technology basis (i.e. same superconductor and structure materials) as that in ITER-CDA. Table 3.2 shows the design parameters chosen for TF magnet of high-A reactor and comparison with TF magnet of ITER-CDA. The critical current density is a key design value and based on the superconducting characteristics given by Fig. 3.1, which are the best performances obtained in laboratory scale experiments and expected to be commercially available during EDA. In ITER-CDA, the critical current density of around 830 A/mm^2 was selected for TF magnet at the maximum magnetic filed of 11.2 T. In case of high-A reactor, the maximum magnetic field is increased up to 13.5 T, resulting in lower current density of around 580 A/mm^2 In addition, high-A reactor requires higher Ampare-turn than ITER-CDA so that the conductor length required for TF magnet of high-A reactor is roughly twice of that of ITER-CDA.

As for structural design, the electromagnetic hoop forces acting on TF magnet of high-A reactor are roughly twice as high as for ITER-CDA: this requires thicker coil case with a thickness of 595 mm in order to keep the maximum stress below the allowable value of 800 MPa. As a result, the cost of TF magnet of high-A reactor increases by about 50% due to doubled conductor length and coil case thickness. Furthermore, higher AC losses due to thick coil case are induced in ranging from factor 2 to 4, which causes the remarkable increase in the cryogenic system capacity.

3.2 Overall Machine Size and Toroidal Field Ripple

The overall configuration of high-A reactor is developed according to the same design philosophy as that of ITER-CDA and the elevation view obtained is shown in Fig. 3.2 together with the ITER-CDA configuration. In high-A reactor, the total volume of reactor structures located inside

the cryostat is increased by about 6% with increasing in major radius from 6 m to 6.6 m, but the in-vessel space inside the vacuum vessel is decreased by 14% due to the small machine height and thick TF coil case, and hence is less desirable for the remote maintenance of in-vessel components such as divertor plates and blanket modules.

Figure 3.3 shows the corresponding radial built of high-A reactor and ITER-CDA. As mentioned previously, TF magnet of high-A reactor is very thick compared with ITER-CDA so as to provide higher magnetic field and to support electro-magnetic forces. The inner diameter and thickness of center solenoid in high-A reactor is larger than those of ITER-CDA, resulting in higher volt-second capability for better plasma operation and longer life time due to low stress on the coil winding. The nuclear shielding capability of high-A reactor is maintained to be the same as that of ITER-CDA.

It is well known that the ripple trapped loss P_{ripple} strongly depends on the aspect ratio and the relation is simply represented by the following scaling,

$$P_{ripple} \propto \delta_0^2 A^4 \qquad (3\text{-}1)$$

where δ_0 is toroidal field ripple at plasma edge and A is aspect ratio. Accordingly, the toroidal field ripple of high-A reactor should be reduced so as to keep the ripple trapped loss at the same level of ITER-CDA. Figure 3.4 shows the relation of δ_0 to the distance between plasma edge and TF winding center as a function of number of TF magnets. Based on the simple scaling and Fig. 3.4, it is decided that the toroidal field ripple of high-A reactor is to be about 0.6% and the distance between plasma edge and TF winding center is increased by 0.8 m compared with ITER-CDA.

3.3 In-vessel Component Maintenance

The segmentation and replacement scheme of in-vessel components such as divertor plates and blanket modules are investigated for high-A reactor. As a result, high-A reactor has less space for handling the in-vessel components and the following difficulties are observed.

(1)The in-board blanket can be segmented into two modules per sector but can not be replaced without out-board blanket removal(see Fig. 3.5). In ITER-CDA, independent replacement of in-board or out-board blanket modules can be possible, so that flexible maintenance scheme and high availability of machine operation are expected.

(2)The divertor plate can be segmented into two modules per sector as same as ITER-CDA. However, the divertor module replacement is rather marginal due to tight space and very accurate posture control

within few 10 mm is required(see Fig. 3.6). In addition, the divertor module becomes wide due to increase in major radius and maintenance ports with a 1.5 m width is at least required for divertor module transportation; this requires grooving of the side wall of the corresponding blanket side module.

As for the structural design of the in-vessel components, the electro-magnetic loads during plasma disruption are essential. In high-A reactor, the plasma current is decreased down to 15 MA but the toroidal field on axis is increased up to 7.2 T. As a result, the electro-magnetic loads generated by coupling between plasma current and toroidal magnetic field are roughly the same as ITER-CDA and no substantial benefit has been observed in the structural design.

3.4 Other Key Features

(1)Neutron wall loading

The neutron wall loading profile depends on aspect ratio and the peaking factor(Pf) defined by the ratio of the maximum wall loading to the average value in poloidal circumference is represented by

$$P_f \propto A^{-0.45} \qquad (3\text{-}2)$$

In case of ITER-CDA, the peaking factor of neutron wall loading is about 1.6 and the maximum wall loading is obtained at the horizontal port region where the blanket test module is install and tested. When the minimum wall loading required for the blanket test module is specified to be 1 MW/m^2, the average wall loading is at least 0.62 MW/m^2 in case of ITER-CDA.

On the other hand, the peaking factor of high-A reactor is estimated to be around 1.4 from the simple scaling mentioned above. Accordingly, the neutron wall loading at the test region is decreased by 15% for the same average value as ITER-CDA and 15% increase in the average value is needed for high-A reactor.

(2)Tritium breeding ratio

In case of high-A reactor, the major radius is increased but the total surface area facing to plasma is decreased by about 10%. because of decrease in minor radius and increase in port opening area. As a result, the tritium breeding ration would be decreased by 10 % when the breeding blanket capability is comparative with that in ITER-CDA.

Table 3.1 Major parameters of High-A reactor compared with ITER CDA

Parameters	High-A	ITER-CDA
Major radius	6.6 m	6.0 m
Minor radius	1.74 m	2.15 m
Aspect ratio	4	3
Plasma current	15 MA	22 MA
Toroidal field on axis	7.18 T	4.85 T
Max. toroidal field	13.5 T	11.2 T

Table 3.2 Design parameters of TF coils for ITER CDA & High-A

		ITER	High-A
Maximum Magnetic	(T)	11.2	13.5
Current Density of Winding	(A/mm^2)	33.9	23.7
Ic/Iop		2.39	2.39
Jc (SC) at Operating Field	(A/mm^2)	830	580
Size of Winding			
Wr	(mm)	307	690
Wt	(mm)	849	880
Total Conductor length	(km)	9.6	18.2
Ampare-turn/coil	(MAT)	9.1	14.4
Centering Force/Coil	(MN)	476	671
Hoop Force/Coil (MN)		1024	2078
Thickness of Outer Ring for the Wedging	(mm)	287.5	595
Compressive Stress of the Outer Ring for the Wedging by Cylinder Model	(MPa)	-416	-426
Maximum Tresca Stress by FEM Analysis	(MPa)	650	⇐
Allowable Stress Limit: Sm	(MPa)	800	⇐

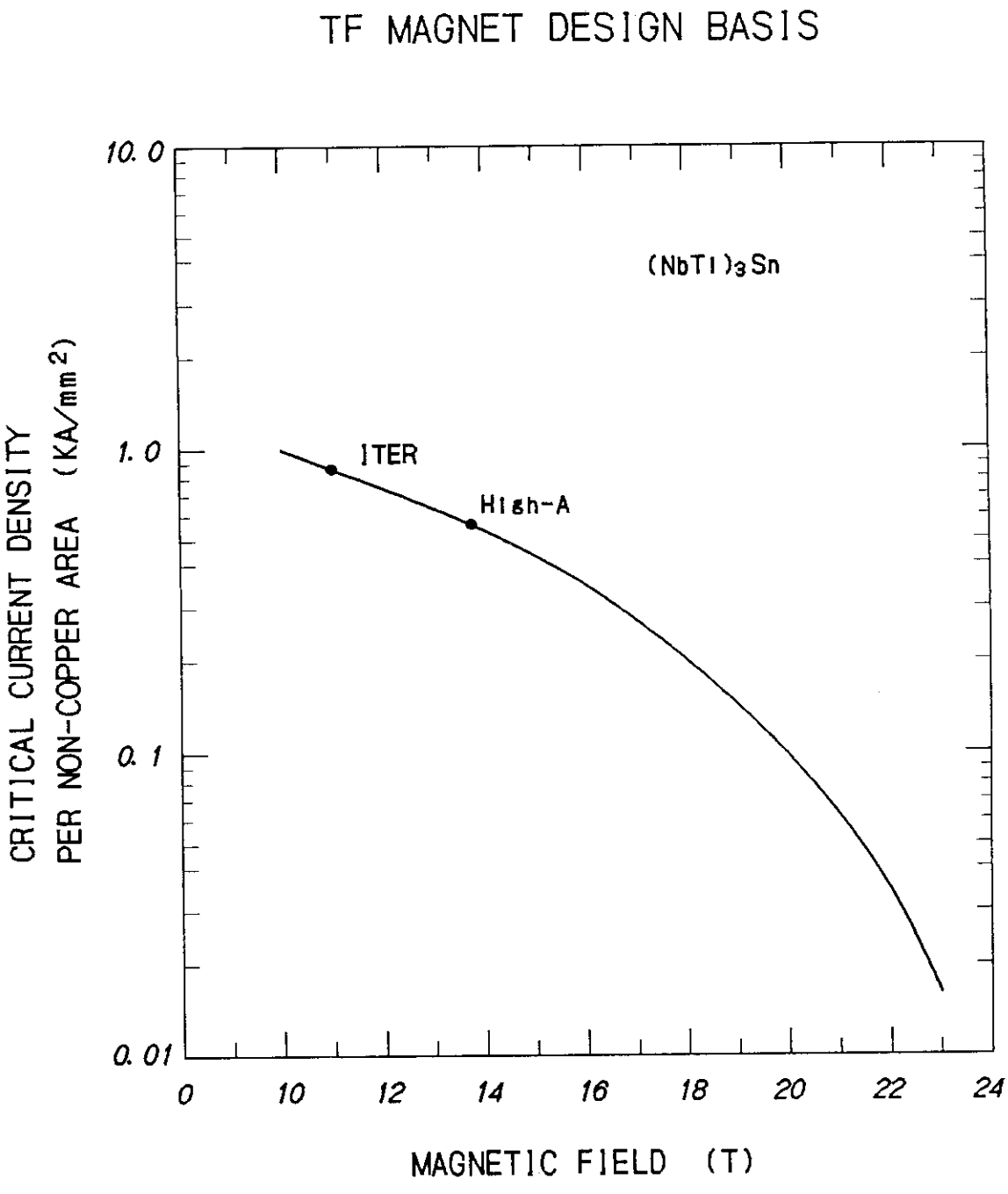

Fig. 3.1 Design basis of toroidal field magnet

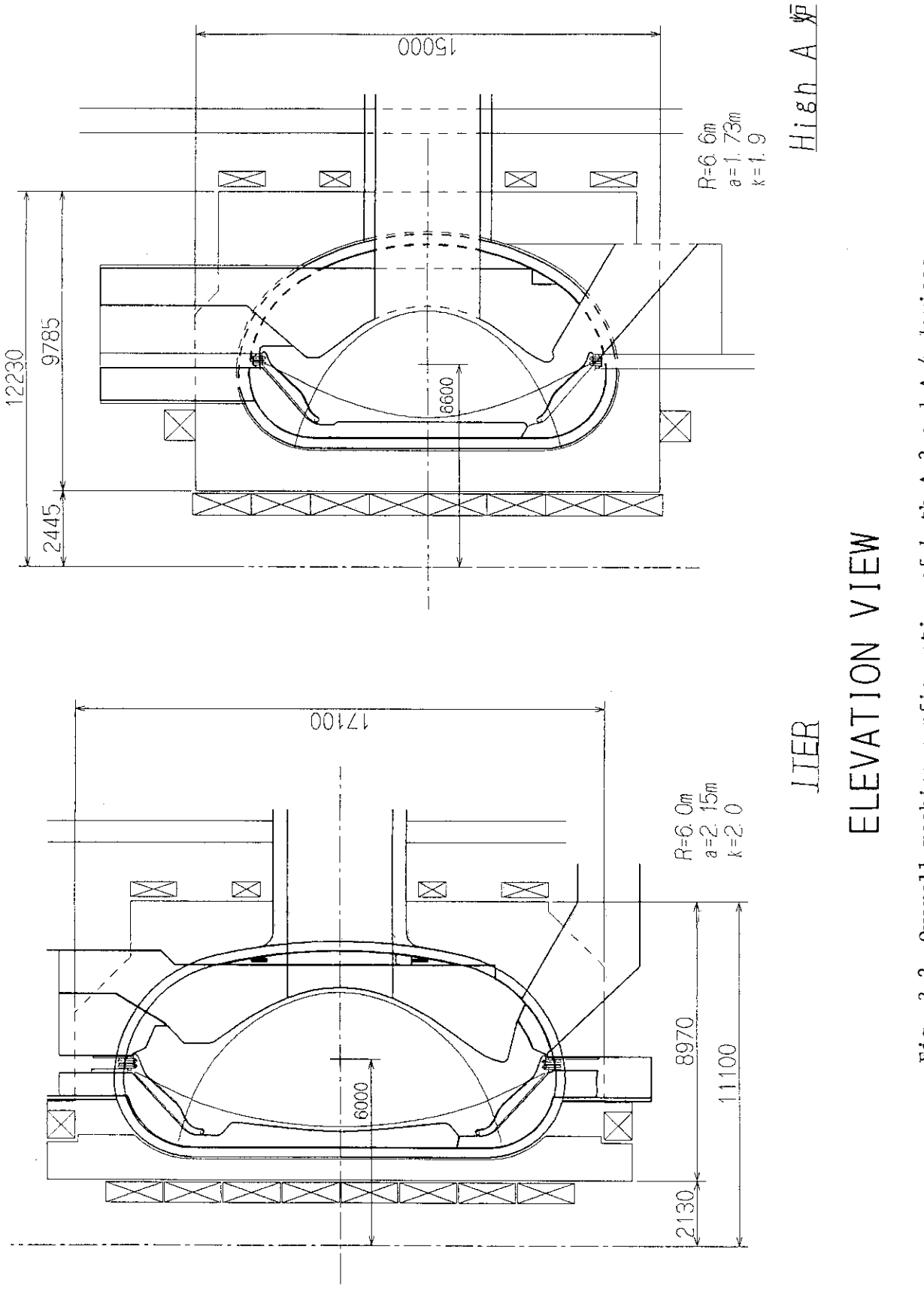

Fig. 3.2 Overall machine configuration of both A=3 and A=4 devices

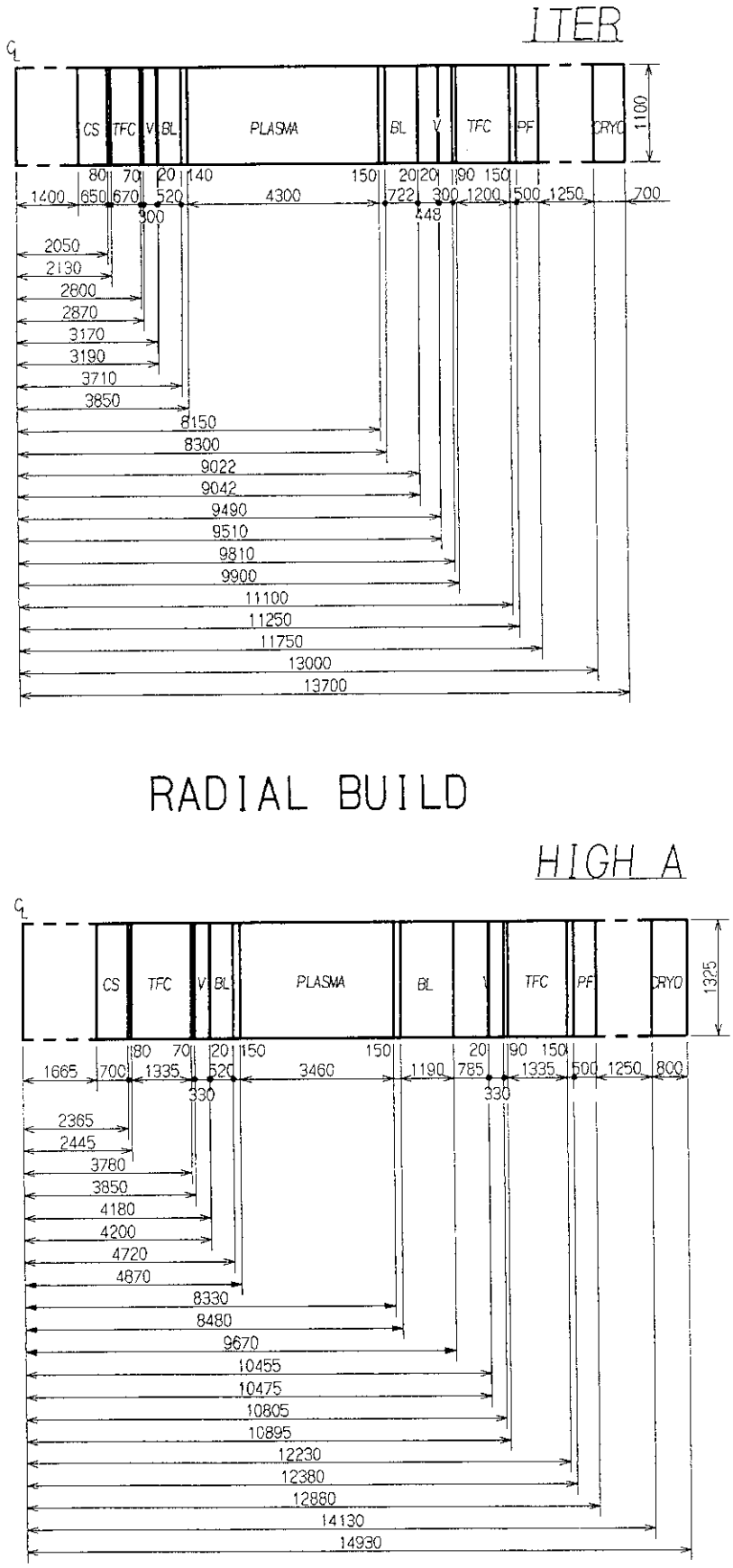

Fig. 3.3 Radial build of A=3 and A=4 devices

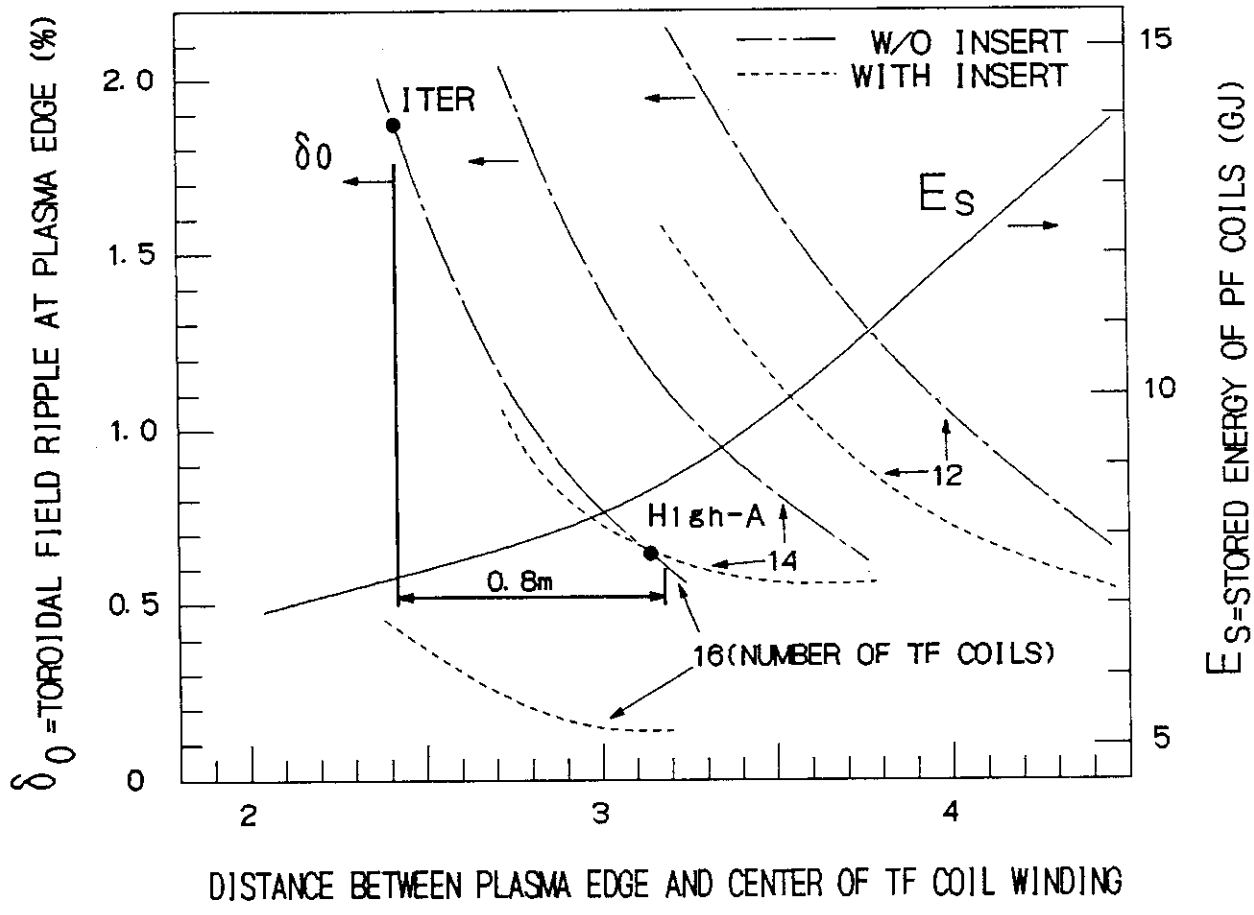

Fig. 3.4 Relation between toroidal field ripple and distance from plasma edge to TF winding center

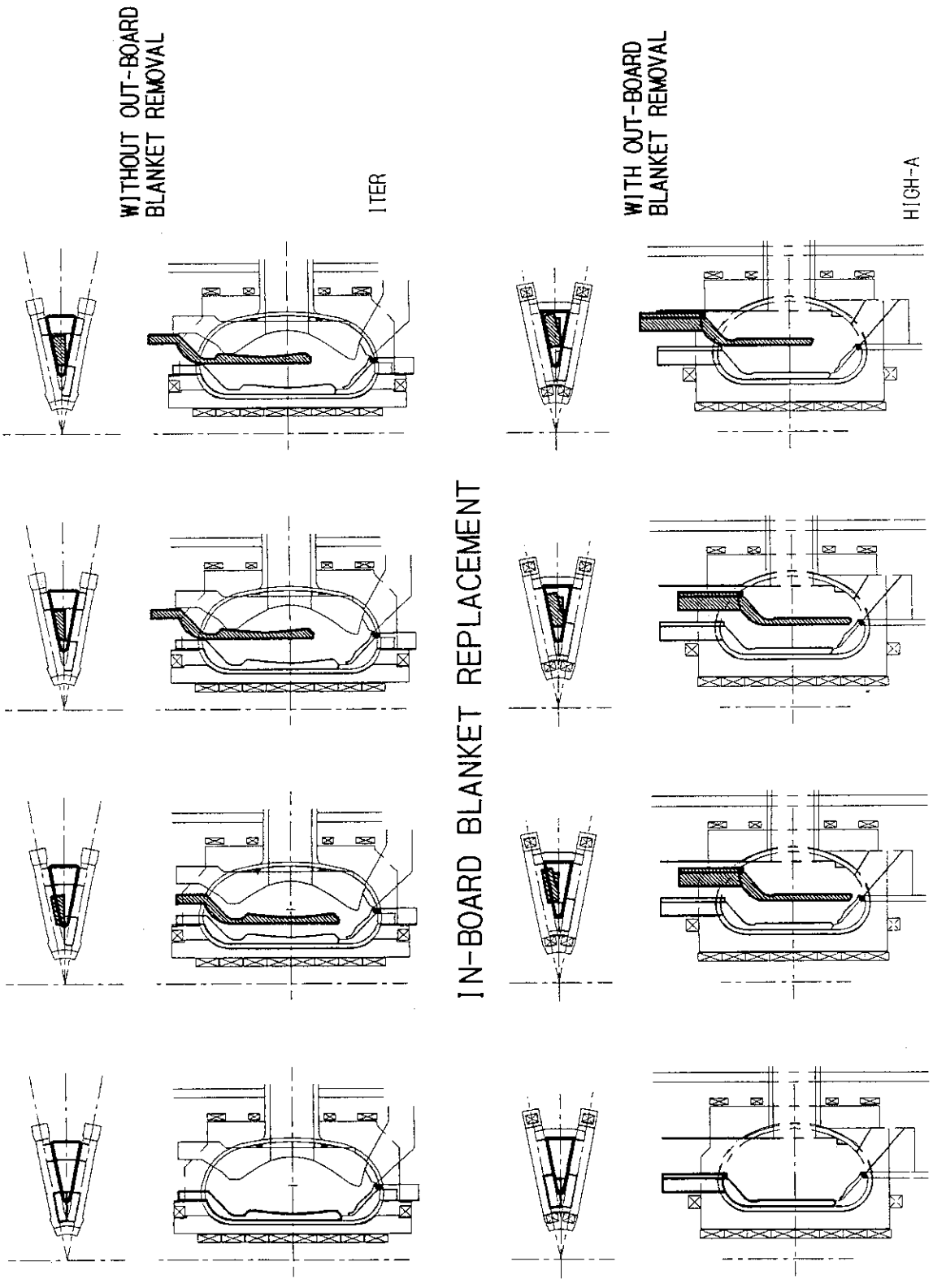

Fig. 3.5 Maintenance scheme of blanket modules for A=3 and A=4 devices

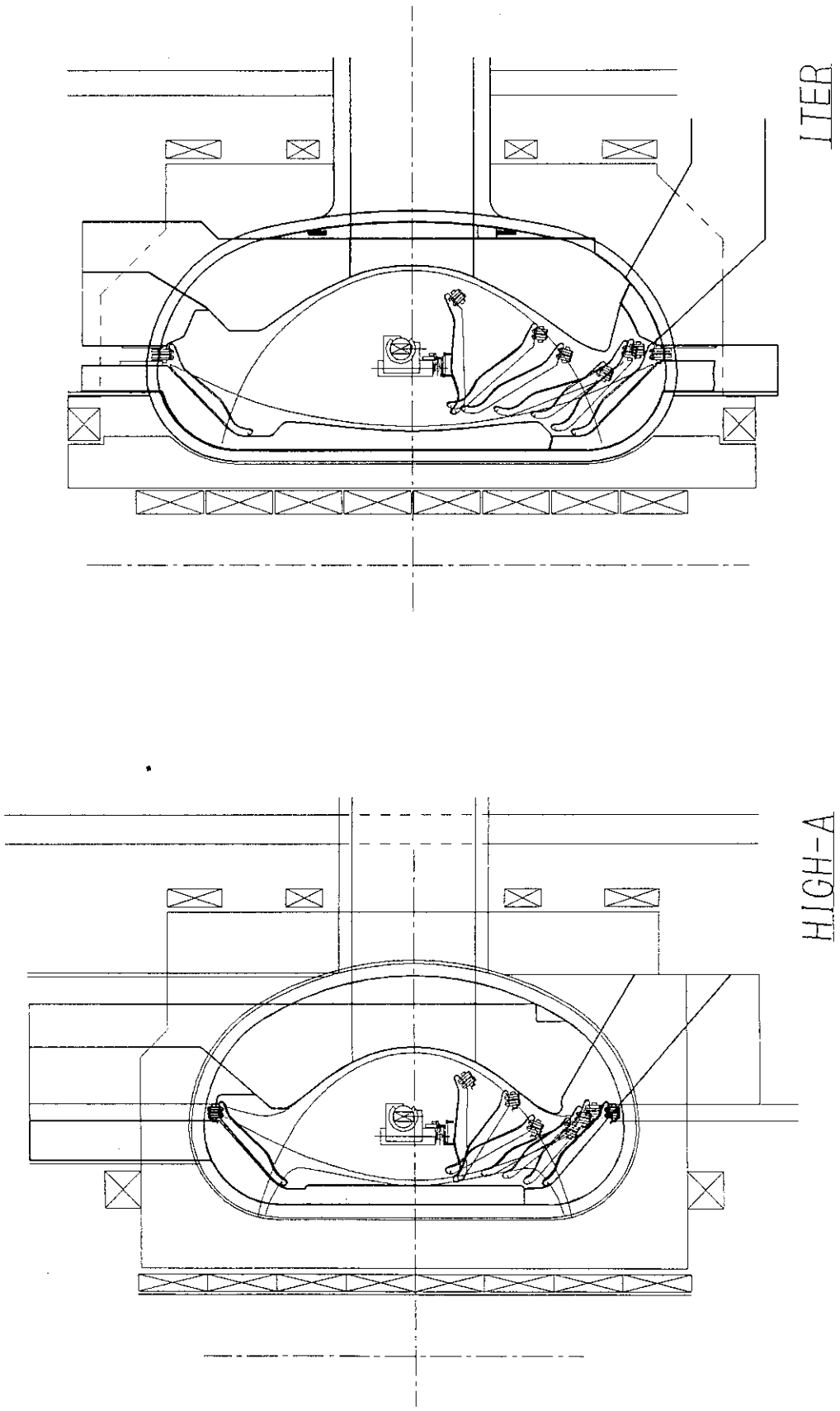

Fig. 3.6 Divertor in-vessel replacement for A=3 and A=4 devices

4. Summary

Comparative study on the plasma performance and the engineering characteristics of low and high aspect ratio devices for ITER design option is done to examine quantitatively the expected merit and demerit of high aspect ratio device on steady state operation. Device parameters of A=3 and 4 are chosen for comparative study based on ITER-power law scaling with providing same ignition performance. Improvement of plasma performance in steady state operation is found very moderate (Q and bootstrap fraction increased by about 1 and 10%, respectively, when A is increased from 3 to 4). Stability margin in vertical instability decreases by about 20% in A=4 device compared with A=3 device. Plasma elongation must be decreased from 2 down to about 1.8 to recover this reduction of stability margin. If such lower elongation should be employed, single null divertor configuration is to be employed to reduce the capacity of poloidal field system. Detailed 2D divertor code calculation shows that peak heat load per unit area of A=4 device is reduced by only 20% when DN divertor configuration could be employed, while with SN configuration it increases, on the contrary, compared with A=3 device with DN configuration. Large experimental capability to obtain the data base for demo-reactor (e.g., high Q with high bootstrap fraction) can be expected even in A=3 device when the extended plasma performance could be realized. Similar overall performance in the future commercial reactor is possible even in A=3 device compared with A=4 device (e.g., SSTR, ARIES-1) by adjusting the fusion power.

In addition, no substantial benefit of engineering features has been observed for A=4 device. According to higher magnetic field requirements, the conductor length and coil case thickness are roughly doubled. The in-vessel space of A=4 device is decreased, resulting in no independent of blanket modules and marginal divertor in-vessel handling. The electromagnetic loads acting on in-vessel components are not reduced because of increase in toroidal magnetic field.

Based on these examinations, it is concluded that high aspect ratio device has not remarkable advantage than low aspect ratio device, and the latter device has similar capability for the prospect of future commercial reactor as the former device. The summary of this comparative study on physics and engineering aspects is listed in an attached appendix. When the scaling has much stronger dependence on A such as H-mode scaling, the advantage of high A device will be more pronounced. Further Physics R&D on confinement scaling, especially A dependence, is fairly important to draw final conclusion.

Acknowledgement

We are grateful to Dr. M. Kikuchi for fruitful discussions and critical comments. He has also pointed out the importance in increasing the fusion power to attain the same bootstrap fraction in low A power reactor. We also thank Dr. N. Ueda for useful discussions on the UEDA code calculations.

References

[1] ITER CDA Team, "ITER Conceptual Design Report", IAEA, Vienna, 1991 and J. Perkins, W. Spears, J. Galambos, H. Iida etal., " ITER Parameter Analysis and Operational Performance. Gilleland, R. H. Bulmer, D. T. Blackfield et al., UCRL-ID-104178 (1990).

[2] INTOR Group, "International Tokamak Reactor", Phase Two A Part III, IAEA, Vienna (1988).

[3] M. F. A. Harrison, A. Kukushkin, ITER-IL-PH-13-9-E-12 (1989).

[4] M. Sugihara, T. Mizoguchi, A. Hatayama, K. Shinya, S. Yamamoto et al., JAERI-M87-108 (1987) (in Japanese).

[5] N. Ueda et al, Nuclear Fusion 28 (1988) 1183.

[6] Y. Shimomura, J. Wesley, A. Astapkovich, L. Bottura, S. Chiocchio et al., "ITER Poloidal Field System', IAEA/ITER/DS/27, IAEA, Vienna, 1991.

[7] Y. Seki, M. Kikuchi, T. Ando, Y. Ohara, S. Nishio et al., 13th Inter. Conf. Plasma Physics and Contr. Nucl. Fusion Res., Washington (1990) IAEA-CN-53/G-1-2.

[8] R. W. Conn et al., ibid, IAEA-CN-53M-1-4.

Acknowledgement

We are grateful to Dr. M. Kikuchi for fruitful discussions and critical comments. He has also pointed out the importance in increasing the fusion power to attain the same bootstrap fraction in low A power reactor. We also thank Dr. N. Ueda for useful discussions on the UEDA code calculations.

References

[1] ITER CDA Team, "ITER Conceptual Design Report", IAEA, Vienna, 1991 and J. Perkins, W. Spears, J. Galambos, H. Iida etal., " ITER Parameter Analysis and Operational Performance. Gilleland, R. H. Bulmer, D. T. Blackfield et al., UCRL-ID-104178 (1990).

[2] INTOR Group, "International Tokamak Reactor", Phase Two A Part III, IAEA, Vienna (1988).

[3] M. F. A. Harrison, A. Kukushkin, ITER-IL-PH-13-9-E-12 (1989).

[4] M. Sugihara, T. Mizoguchi, A. Hatayama, K. Shinya, S. Yamamoto et al., JAERI-M87-108 (1987) (in Japanese).

[5] N. Ueda et al, Nuclear Fusion 28 (1988) 1183.

[6] Y. Shimomura, J. Wesley, A. Astapkovich, L. Bottura, S. Chiocchio et al., "ITER Poloidal Field System', IAEA/ITER/DS/27, IAEA, Vienna, 1991.

[7] Y. Seki, M. Kikuchi, T. Ando, Y. Ohara, S. Nishio et al., 13th Inter. Conf. Plasma Physics and Contr. Nucl. Fusion Res., Washington (1990) IAEA-CN-53/G-1-2.

[8] R. W. Conn et al., ibid, IAEA-CN-53M-1-4.

Appendix:Pros and Cons of High Aspect Ratio Design

	Issue	Key Issues	Pros/Cons
1	Steady State Operation	Bootstrap current	increase by ~10% for $P_w < 1 MW/m^2$ Resultant increase of Q is ~1.
		Divertor heat load	DN: decreases SN: more than in ITER
		Impurity	can be reduced due to possible increase in plasma density (~15% increase in n_e). The increase in n_e is favorable for the remote radiative cooling.
2	Reliability & Flexibility of plasma operation	Energy confinement	Present H-mode scaling suggests a favorable direction for high A or large R. More detailed assessment is needed.
		Operational flexibility	Worse (See 3 &4) Difficulty in plasma control by a short time scale (~sec) due to the increase in the AC loss.
		Operational space	Narrow due to synchrotron radiation. Needs high reflection by wall.
		V.s capability Reliability of the central solenoid	372V.s and 122 V.s for burn in JP-HARD while 330 V.s and 45 V.s in ITER. Better
3	Vertical stability	Stability margin	Reduced (~20% reduction for κ=2). For A=4, elongation should be reduced down to κ=1.8 to keep the same stability margin.

4	Poloidal field system	Stored energy	increase. DN: 22GJ for κ=1.9 and 60GJ for κ=1.8. SN: 12GJ while 12GJ for DN in ITER. The increase in the stored energy reduces the operational flexibility due to increase in AC loss and the difficulty in the separatrix sweep, and leads to the increase in the capacity of the power supply and cooling system.
5	Toroidal coil	Size and cost	increase. For 13.5T and 240A/mm^2 the same technology as assumed in ITER (11.4T and 347A/mm^2) is applicable. The necessary length of the conductor is about twice longer than that in ITER.
		Stress and force	increase (See discussion in Engn. sub-group).
		Ripple loss	increase for the same ripple value ($\sim A^4\delta^2$). The increase in the outer leg is needed.
6	Current drive	ICRF	15% increase for JP-HARD due to the reduction of trapped electrons.
		ECH	Development of 180GHz technology is needed.
7	Maintenance	Blanket module	The removal of outer modules is needed before the removal of the inner modules.
		Divertor plates	Marginal

8	Vacuum vessel	Loop resistance	can be decreased down to 4μΩ, while it cannot be employed due to the requirement for plasma control.
9	Effect of disruption	Plasma magnetic energy Force	decreases as I_p^2 (which reduces the energy of runaway electrons). cst. for $B_t x I_p$.
10	Neutron wall load	Intensity at the test area	ITER(A=2.8):1.6x average value INTOR(A=4):1.3x average value The average intensity should be increased by 15% for A=4.
11	Tritium breeding	Breeding ratio	The area is almost constant. The breeding ratio is reduced (~10%) by the reduction of the plasma minor radius.
12	Machine size	Vertical stability, Divertor performance, TF ripple loss	US-HARD: κ=2.0, δ=0.45, R=6m, a=1.6m JP-HARD: κ=1.9, δ=0.35, R=6.5m, a=1.7m SU-HARD: κ=1.85, δ= , R= m, a= m
13	Projection to DEMO	Steady state operation Flexibility in experiments	Better. However the most critical issue is the divertor problems and a serious improvement is questionable in HARD. The ITER design is more flexible than HARD in vertical stability, PF system and the maintenance. The synchrotron radiation is a critical issue for the operation space in HARD.